Atmos. Chem. Phys., 23, 15561–15587, 2023
https://doi.org/10.5194/acp-23-15561-2023

Atmospheric Chemistry and Physics
Open Access
EGU

Marine carbohydrates in Arctic aerosol particles and fog – diversity of oceanic sources and atmospheric transformations

Sebastian Zeppenfeld[1], Manuela van Pinxteren[1], Markus Hartmann[2], Moritz Zeising[3], Astrid Bracher[3,4], and Hartmut Herrmann[1]

[1]Atmospheric Chemistry Department (ACD), Leibniz Institute for Tropospheric Research (TROPOS), Leipzig, Germany
[2]Atmospheric Microphysics (AMP), Leibniz Institute for Tropospheric Research (TROPOS), Leipzig, Germany
[3]Alfred Wegener Institute Helmholtz Centre for Polar and Marine Research, Bremerhaven, Germany
[4]Institute of Environmental Physics, University of Bremen, Bremen, Germany

Correspondence: Hartmut Herrmann (herrmann@tropos.de)

Received: 18 July 2023 – Discussion started: 25 July 2023
Revised: 2 October 2023 – Accepted: 9 November 2023 – Published: 20 December 2023

Abstract. Carbohydrates, originating from marine microorganisms, enter the atmosphere as part of sea spray aerosol (SSA) and can influence fog and cloud microphysics as cloud condensation nuclei (CCN) or ice-nucleating particles (INP). Particularly in the remote Arctic region, significant knowledge gaps persist about the sources, the sea-to-air transfer mechanisms, atmospheric concentrations, and processing of this substantial organic group. In this ship-based field study conducted from May to July 2017 in the Fram Strait, Barents Sea, and central Arctic Ocean, we investigated the sea-to-air transfer of marine combined carbohydrates (CCHO) from concerted measurements of the bulk seawater, the sea surface microlayer (SML), aerosol particles and fog. Our results reveal a wide range of CCHO concentrations in seawater (22–1070 $\mu g\,L^{-1}$), with notable variations among different sea-ice-related sea surface compartments. Enrichment factors in the sea surface microlayer (SML) relative to bulk water exhibited variability in both dissolved (0.4–16) and particulate (0.4–49) phases, with the highest values in the marginal ice zone (MIZ) and aged melt ponds. In the atmosphere, CCHO was detected in super- and submicron aerosol particles ($CCHO_{aer,super}$: 0.07–2.1 $ng\,m^{-3}$; $CCHO_{aer,sub}$: 0.26–4.4 $ng\,m^{-3}$) and fog water ($CCHO_{fog,liquid}$: 18–22 000 $\mu g\,L^{-1}$; $CCHO_{fog,atmos}$: 3–4300 $ng\,m^{-3}$). Enrichment factors for sea–air transfer varied based on assumed oceanic emission sources. Furthermore, we observed rapid atmospheric aging of CCHO, indicating both biological/enzymatic processes and abiotic degradation. This study highlights the diverse marine emission sources in the Arctic Ocean and the atmospheric processes shaping the chemical composition of aerosol particles and fog.

1 Introduction

Sea spray aerosol (SSA) represents one of the major aerosol species in the lower troposphere over the remote Arctic Ocean, particularly during the spring and summer months in the Northern Hemisphere (Chi et al., 2015; Hara et al., 2003; Kirpes et al., 2018; May et al., 2016). Depending on the size distribution and chemical composition, SSA particles strongly contribute to the populations of cloud condensation nuclei (CCN) and ice-nucleating particles (INP) affecting the polar radiative budget through the formation of liquid droplets and ice crystals in fog and clouds (DeMott et al., 2016; Lawler et al., 2021; McCluskey et al., 2018; Penner et al., 2001; Schiffer et al., 2018; Wilbourn et al., 2020). Notably in the Arctic, one of the regions most affected by global warming, there is still a lack of knowledge about the

relationship between the formation and evolution of clouds and specific chemical properties of SSA particles (Wendisch et al., 2023).

SSA is emitted directly from the ocean surface through wind-driven processes and, as a consequence, contains the salts and the organic matter (OM) present in seawater, including carbohydrates (CHO) as one of the largest identified organic fractions (Quinn et al., 2015, and references therein). In microalgae, bacteria and also more complex marine organisms (e.g., kelp, krill), carbohydrates have important metabolic, structural and protective functions or are released in response to environmental stress, such as freezing or lack of nutrients (Krembs et al., 2002; Krembs and Deming, 2008; McCarthy et al., 1996; Mühlenbruch et al., 2018; Suzuki and Suzuki, 2013; Wietz et al., 2015). In seawater, most carbohydrates appear as linear or branched oligo- and polysaccharides, commonly referred to as combined carbohydrates (CCHO). They can be found in both dissolved (*d*CCHO) and particulate (*p*CCHO) phases, distinguished operationally by a 0.2 µm filtration. These macromolecules consist of several monosaccharides, such as hexoses, pentoses, deoxy sugars, amino sugars, uronic acids and amino sugar acids, which are connected via glycosidic bonds (Benner and Kaiser, 2003; Engel and Händel, 2011; Panagiotopoulos and Sempéré, 2005). Most CCHO are quite stable within the marine environment unless they are either hydrolyzed in the presence of specific enzymes or in a very acidic setting (Arnosti, 2000; Panagiotopoulos and Sempéré, 2005). Heterotrophic bacteria use extracellular enzymes to selectively degrade CCHO into absorbable shorter molecules leaving a certain part as recalcitrant, more persistent OM (Alderkamp et al., 2007; Becker et al., 2020; Goldberg et al., 2011; Wietz et al., 2015). While *p*CCHO is mostly attributed to recent productions by local phytoplankton indicated by high positive correlations with total chlorophyll *a* (TChl *a*), *d*CCHO appears to be the result of more complex metabolic and transformation processes after its release (Becker et al., 2020; Fabiano et al., 1993; Goldberg et al., 2011; Zeppenfeld et al., 2021a). In contrast, dissolved free carbohydrates (*d*FCHO), short sugars in their monomer form, are quickly consumed by marine microorganisms resulting in much lower concentrations of *d*FCHO compared to CCHO in ambient seawater (Engbrodt, 2001; Engel and Händel, 2011; Ittekkot et al., 1981; Zeppenfeld et al., 2020).

In the remote marine atmosphere, carbohydrates are suggested to significantly impact cloud properties by contributing to both the CCN and INP populations (Alpert et al. 2022; Leck et al., 2013; Orellana et al., 2011; van Pinxteren et al., 2022). Carbohydrates appear both in super- and submicron SSA particles (Aller et al., 2017; Leck et al., 2013; Russell et al., 2010; Zeppenfeld et al., 2021a), most likely resulting from their emission from the surface of the ocean after bubble bursting as part of jet and film droplets (Veron, 2015; Wang et al., 2017). In addition to the bulk surface seawater, the sea surface microlayer (SML) as the uppermost layer of the oceanic water column is an important source of OM, and thus marine carbohydrates, in the SSA. The SML is described as a gelatinous film on top of the ocean, which is often enriched in surface-active substances or buoyant gel particles compared to the underlying bulk water (Engel et al., 2017; Wurl et al., 2009, 2011; Zäncker et al., 2017). Entrained air bubbles rise within the upper part of the water column collecting surface-active organics on the bubble surfaces from the bulk seawater (Burrows et al., 2014). Eventually they pass the thin SML and burst there, releasing film and jet droplets containing a mixture of substances found within the bulk water and the SML (Burrows et al., 2014). At the same time, surfactants, exopolymers and microgels in the SML increase the stability of the cap films of the bubbles, extend their lifetimes and enable the drainage of water-soluble compounds (Bigg and Leck, 2008; Bikerman, 2013; Sellegri et al., 2006). Consequently, the sea–air transfer occurs in a chemo-selective manner leading to a strong size-dependent enrichment of surface-active organics relative to water-soluble sodium (Na^+) and, hence, a relative chemical composition of SSA different to the surface seawater (Facchini et al., 2008; O'Dowd et al., 2004; van Pinxteren et al., 2017; Prather et al., 2013; Quinn et al., 2015; Triesch et al., 2021a, b). These chemo-selective enrichments of organic substances in the SSA relative to bulk water, especially in the submicron size range, usually exceed the enrichments in the SML by orders of magnitude (van Pinxteren et al., 2017; Schmitt-Kopplin et al., 2012). The underlying mechanisms for the chemo-selective sea–air transfer of carbohydrates, including co-adsorption, are complex and subject of several recent and ongoing laboratory tank and modeling studies (Burrows et al., 2016; Hasenecz et al., 2020; Schill et al., 2018; Xu et al., 2023). After their emission, fresh SSA particles, including the contained carbohydrates, undergo atmospheric aging due to a not yet well-understood interplay of several atmospheric processes, such as atmospheric acidification, abiotic radical chemistry, and biological and enzymatic modifications (Angle et al., 2021; Hasenecz et al., 2020; Malfatti et al., 2019; Trueblood et al., 2019; Zeppenfeld et al., 2021a), potentially also altering their microphysical properties.

Besides SSA, high concentrations of marine carbohydrates in fog and low-level clouds in the marine environment are plausible due to the high hygroscopicity of SSA serving as good CCN (Xu et al., 2022) transferring OM from the particle into the liquid phase, the high water-solubility of carbohydrates, and cloud-borne microorganisms potentially forming carbohydrates in situ (Matulová et al., 2014). Only a few studies conducted at field sites exposed to marine air masses measured certain subgroups of carbohydrates, such as primary saccharides (Dominutti et al., 2022) or transparent exopolymer particles (TEPs) (Orellana et al., 2011; van Pinxteren et al., 2022) so far in fog/clouds. However, the sources of marine carbohydrates in marine ambient fog/clouds, including $d\mathrm{FCHO}_{\mathrm{fog}}$ and $\mathrm{CCHO}_{\mathrm{fog}}$, and their relationship to

the bulk seawater, SML and aerosol particles still lack elucidation.

During the summer months, the chemical compounds of natural SSA and marine fog can be studied in the Arctic Ocean due to the low influence of long-range transported anthropogenic pollution (Bozem et al., 2019; Schmale et al., 2021). However, the presence and seasonal evolution of Arctic sea ice divides this pristine region into a complex ensemble of several sea-ice-related sea surface compartments. These encompass the open leads – sea ice fractures with variable widths ranging from several to hundreds of meters – and polynyas, which are larger, more persistent areas of open water within the pack ice. Furthermore, there is the ice-free ocean, the marginal ice zone (MIZ) defined by a sea ice concentration threshold between 15 % and 80 % (Rolph et al., 2020), and melt ponds forming and developing during the melting season on top of the ice floes. These environments are characterized by different chemical, physical and biological characteristics potentially influencing the quantity and properties of the SSA emitted. Recent studies observed, for instance, that the number and efficiency of Arctic INP are strongly dominated by the type of sea-ice-related sea surface compartments that the air masses had passed before sampling (Creamean et al., 2022; Hartmann et al., 2021; Papakonstantinou-Presvelou et al., 2022; Porter et al., 2022). However, the individual conclusions still appear controversial and might be biased by seasonal and interannual variabilities. Consequently, more systematic studies in the Arctic, also with regard to the chemical properties of the aerosol particles, are required to achieve more conclusive results.

To increase the knowledge about marine carbohydrates as important constituents of SSA and potential CCN and INP, we present here the results of a comprehensive field study conducted onboard the German icebreaker RV *Polarstern* from May to July 2017. We performed concerted measurements of bulk seawater, SML, size-resolved aerosol particles and fog water at different locations dominated by different sea-ice-related sea surface compartments (ice-free, leads and polynyas, MIZ, melt ponds) in the Arctic Ocean. All marine and atmospheric compartments are discussed and compared on absolute CCHO concentrations, calculated CCHO / Na^+ ratios, the relative monosaccharide contribution to CCHO and the occurrence of *d*FCHO. The complex nature of these primary emission mechanisms and subsequent atmospheric aging of marine CCHO in the Arctic Ocean are discussed in relation to our findings. Our Arctic results are collated with those from the Southern Ocean at the Antarctic Peninsula during the austral summer, as presented in Zeppenfeld et al. (2021a) following a similar experimental design. While both polar locations are remote marine regions with comparable meteorological conditions during the sampling periods, the presence of Arctic sea ice adds another dimension of complexity to data interpretation.

2 Experiment

2.1 Study area and field sampling

Field samples were gathered during the PS106 (PASCAL/SiPCA) campaign (Macke and Flores, 2018; Wendisch et al., 2018) conducted from May to July 2017 on board the German icebreaker RV *Polarstern* in the Fram Strait, Barents Sea and central Arctic Ocean, including a period operating from a drifting ice station (3–16 June 2017).

Marine SML and corresponding bulk water samples were collected from various locations as shown in Supplement Fig. S1. These include the ice-free ocean (four sampling events), open water areas within the pack ice (20 sampling events, without distinguishing between open leads and polynyas), the MIZ (five sampling events), and young and aged melt ponds (six sampling events). Using visual characteristics, melt ponds were categorized as young (small, bluish, clear) or aged (larger, darker blue to greenish, and turbid with particulates and microalgae). To minimize contamination from exhausts and wastewater, water samples were taken at distances greater than 100 m from the ship. Seawater was collected either using a rubber boat or directly from the ice edge. SML samples were obtained by immersing a glass plate (length: 50 cm, width: 20 cm, thickness: 0.5 cm, sampling area: 2000 cm^2) vertically into the surface water and slowly withdrawing it at a speed of approximately 15 cm s^{-1} (van Pinxteren et al., 2012; Zeppenfeld et al., 2021a). The adhered SML film was drawn off the glass plate surface into a prewashed wide-neck plastic bottle by a framed Teflon wiper. The average thickness of the SML collected during this field study was 76 ± 10 µm, which was calculated based on the volume of the SML sample collected, the area of the immersed glass plate and the number of dips as described by Cunliffe and Wurl (2014). Despite air temperatures during PS106 (median: −0.5 °C; minimum: −7.6 °C) hovering around or slightly below the freezing point of seawater, the SML remained unfrozen on the glass plate during sampling. The corresponding bulk water was taken from a defined depth of 1 m into LDPE bottles attached to a telescopic rod, except in the bottom closed melt ponds where it was scooped from the bottom at approximately 20–40 cm depth. Whenever melt pond sampling took place, snow samples were collected from the ice floe surface roughly 10 m away from the melt pond. Before each sampling, the sampling containers were first rinsed with a few milliliters of the corresponding aqueous sample which was disposed immediately after. On board, small aliquots of the water samples were analyzed immediately for salinity using a conductivity meter (pH/Cond 3320, WTW), colored dissolved organic matter (CDOM) and particulate absorption (PAB), with more details in Sect. 2.6. For later chemical analyses (inorganic ions, pH, carbohydrates) 500–1000 mL of 0.2 µm filtered water sample (dissolved fraction), 0.2 µm polycarbonate filters (particulate fraction) and field blanks were stored at −20 °C.

The sampling of ambient aerosol particles was conducted at the starboard side of RV *Polarstern* at the top of the observation deck at a height of approx. 25 m above sea level as already described in Kecorius et al. (2019). Size-segregated aerosol particles were sampled in five size ranges (stage 1: 0.05–0.14 µm, stage 2: 0.14–0.42 µm, stage 3: 0.42–1.2 µm, stage 4: 1.2–3.5 µm, stage 5: 3.5–10 µm aerodynamic particle diameter with a 50 % cut-off) on aluminum foils by using two synchronized low-pressure Berner impactors (Hauke, Austria) with a flow rate of 75 L min^{-1} and a sampling time of 3–6 d. To avoid the condensation of atmospheric water and subsequent microbial activities on the aluminum foils, 3 m long heated tubes between the isokinetic inlets and the impactors reduced the relative humidity of the sampled air to 75 %–80 %, when the ambient relative humidity was higher. During this field study, the difference of the temperatures of the ambient air at the inlet and the sampled air after the heating never exceeded 9 K. Consequently, losses of semivolatile compounds or changes by heat-induced chemical reactions are expected to be neglectable. Furthermore, the Berner impactors were thermally insulated by a polystyrene shell. After sampling, the foils were stored in aluminum containers at −20 °C until analysis. In this study, the results from stages 1–3, 4–5 and 1–5 were summed up as submicron (sub), supermicron (super) and PM_{10}, respectively. Details about the size-resolved aerosol particle samples and corresponding meteorological information are given in Table S1 (in total 15 complete sets of Berner foils).

Close to the aerosol sampling, fog was collected using the Caltech Active Strand Cloud Collector Version 2 (CASCC2) as described by Demoz et al. (1996). Bulk fog droplets were impacted on Teflon strands with a diameter of 508 µm and collected into a prewashed Nalgene polyethylene bottle. The flow rate was 5.3 m^3 min, and the 50 % lower cut-off was determined to be approximately 3.5 µm. Further information about the 22 fog samples collected during the PS106 campaign including meteorological information can be found in Table S2 and in Hartmann et al. (2021).

2.2 Total aerosol particle mass concentrations

Before and after sampling, the aluminum foils were equilibrated (3 d, 20 °C, 50 % relative humidity) and weighed using a precise microbalance (Mettler Toledo XP2U, weighing error: ±4.6 µg). Total particle mass concentrations ($mass_{aer,stage\ y}$) were calculated for each Berner stage as the ratio between the difference of the absolute foil masses after and before sampling and the sampled air volume. Afterwards, aluminum foils were divided for further chemical analyses.

2.3 OC / EC in aerosol samples

Organic carbon (OC_{aer}) and elemental carbon (EC) on Berner aerosol foils were determined as described by Müller et al. (2010) using a two-step thermographic method (C/S MAX, Seifert Laborgeräte, Germany) with a nondispersive infrared sensor.

2.4 Carbohydrates in aerosol particles, fog, snow, seawater and melt ponds

Marine carbohydrates in the particulate (pCCHO, > 0.2 µm) and dissolved (dCCHO/dFCHO, < 0.2 µm) phases, including truly dissolved molecules and small colloids, were quantified from seawater and melt pond samples following the protocol presented by Zeppenfeld et al. (2020, 2021a) using high-performance anion-exchange chromatography with pulsed amperometric detection (HPAEC-PAD) equipped with a Dionex CarboPac PA20 analytical column (3 mm × 150 mm) and a Dionex CarboPac PA20 guard column (3 mm × 30 mm). The monosaccharides fucose (Fuc), rhamnose (Rha), arabinose (Ara), galactose (Gal), glucose (Glc), xylose (Xyl), mannose (Man), fructose (Fru), galactosamine (GalN), glucosamine (GlcN), muramic acid (MurAc), galacturonic acid (GalAc) and glucuronic acid (GlcAc) were identified by their retention times. dFCHO represents the sum of identifiable monosaccharides before, and dCCHO and pCCHO additionally released after an acid hydrolysis (0.8 M HCl, 100 °C, 20 h). CCHO is the sum of dCCHO and pCCHO. CHO represents the sum of CCHO and dFCHO and consequently encompasses all carbohydrates measured within this study. Figure 1 gives an overview of the carbohydrate-related abbreviations used here. Marine carbohydrates in fog water, snow and extracts from size-resolved aerosol particles were measured with ($CCHO_{fog}$, $CCHO_{aer}$) or without ($d$$FCHO_{fog}$, $d$$FCHO_{aer}$) prior acid hydrolysis.

2.5 Sodium and pH in aerosol particles, fog, seawater and melt ponds

Major inorganic ions, including sodium (Na^+), were determined from 0.45 µm filtered aqueous extracts of the size-resolved aerosol samples (50 % of the Berner foil in 2 mL ultrapure water), fog water, diluted (1 : 15 000) seawater and melt pond samples using ion chromatography (ICS-3000, Dionex) as described by Müller et al. (2010). In this study, we discuss the results for Na^+ as a proxy for SSA emissions in remote marine regions. Additionally, the pH was monitored by an additional autosampler sample conductivity and pH accessory (Dionex) in all seawater, melt pond and, whenever enough sample volume was available, in fog water.

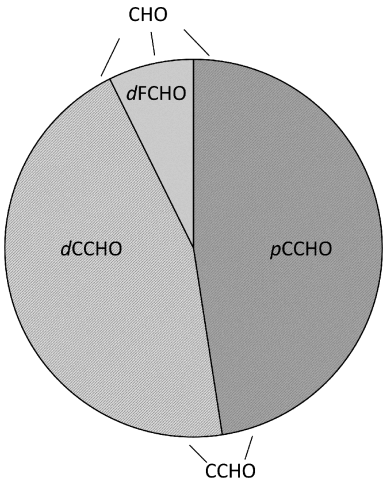

Figure 1. Overview of the abbreviations for carbohydrates (CHO) in seawater. CCHO: combined carbohydrates; *p*CCHO: particulate combined carbohydrates, *d*CCHO: dissolved combined carbohydrates; dFCHO: dissolved free carbohydrates.

2.6 Absorption by phytoplankton, non-algal particles and colored dissolved organic matter in seawater and melt pond samples

For the investigation of bio-optical parameters in seawater and melt pond samples, the particulate fraction was collected by filtering the water samples (5–500 mL) onto glass-fiber filters (GF/F, Whatman), while the dissolved fraction was filtered through 0.2 µm Spartan syringe filters (Whatman, Germany) immediately after sampling. The GF/F filters were analyzed to determine the absorption spectra (i.e., 320–844 nm, 2 nm resolution) using the quantitative filtration technique with an integrative-cavity absorption meter setup (QFT-ICAM) as developed by Röttgers et al. (2016). We followed the protocol by Liu et al. (2018) for the instrument used here and the determination of the absorption coefficients by total particles (a_p440), phytoplankton ($a_{ph}440$) and non-algal particles ($a_{NAP}440$) at $\lambda = 440$ nm.

The absorption for the dissolved fraction ($a_{CDOM}(\lambda)$) between 270 and 750 nm (1 nm resolution) were measured as triplicates using a long-path-length liquid waveguide capillary cell (LWCC) system following the procedure by Lefering et al. (2017) and including the correction for salinity effects by Röttgers et al. (2014) as described for our instrumentation in Álvarez et al. (2022). The absorption coefficients in the visible at 443 nm ($a_{CDOM}443$) and UV at 350 nm ($a_{CDOM}350$) bands were used as indicators of CDOM magnitude.

2.7 Supporting observations

The German research vessel *Polarstern* performs continuous meteorological surface measurements during times of ship operation. For this study, we used the data from the HMP155 thermometer/hygrometer probe (Vaisala), the ultrasonic anemometer (Thies Clima) and the FS11 visibility sensor (Vaisala) installed at a height of 29, 39 and 20 m above sea level, respectively. The quality-controlled data made available by the operators on the public repository PANGAEA (Schmithüsen, 2018, 2019) supported the interpretation of the results of this study.

The 120 h back-trajectories were computed for the sampling periods of the size-resolved aerosol particles and fog water events using the NOAA HYSPLIT model (Stein et al., 2015). The back-trajectories were calculated on an hourly basis using the GDAS1 meteorological fields (Global Data Assimilation System; 1° latitude/longitude; 3-hourly) and at arrival heights of 50, 250 and 1000 m. Sea ice concentration data were retrieved from ERDDAP (Environmental Research Division's Data Access Program), a data server maintained by NOAA (National Oceanic and Atmospheric Administration). The MIZ was defined here as the oceanic region with a sea ice concentration between 15 % and 80 %. Data on melt pond fractions were accessed from the sea ice remote sensing data achieve of the University of Bremen (https://data.seaice.uni-bremen.de, last access: 10 April 2023, Istomina et al., 2020).

2.8 Statistics, calculations and visualization

Statistical analyses, calculations and visualization were performed in OriginPro, Microsoft Excel and R version 4.2.1 using the following packages: oce, ocedata, ncdf4, openair, ggplot2, reshape2, scales, lubridate, cmocean, maps, mapdata, rgdal, raster, RColorBrewer and sp. Time-resolved back-trajectories and sea ice maps were combined using R to compute and visualize the air mass history regarding the sea-ice-related sea surface compartments that have been passed. As a result, relative residence times of the air masses over certain surface features (ice-free, MIZ, pack ice, land) 12 h before sampling were calculated based on defined thresholds for sea ice concentration: less than 15 % for ice-free ocean, 15 %–80 % for MIZ and over 80 % for pack ice. Based on the remote sensing data used, we did not distinguish between open leads and melt ponds as the air traversed the pack ice. Box-and-whisker plots represent the interquartile range (box), median (horizontal line within the box), average (open square), and the minimum and maximum values of the datasets (whiskers). Measured mean values are given together with the calculated standard deviations (±). Correlations between two measured variables were expressed via the Pearson correlation coefficient R. The thresholds of significance were set for the p values 0.1, 0.05, 0.01 and 0.001.

Enrichment factors for CCHO in the SML (EF_{SML}) relative to the corresponding bulk sample in different sea-ice-related sea surface compartments (ice-free, leads and polynyas, MIZ, melt ponds) were calculated based on Eq. (1) with $[x]_{SML}$ and $[x]_{bulk}$ representing the concentrations of either *p*CCHO or *d*CCHO. For the calculation of enrich-

ment factors of CCHO in aerosol particles on Berner stage y ($EF_{aer,stage\ y}$; Eq. 2) and fog water (EF_{fog}; Eq. 3) relative to the bulk water samples, the ocean was assumed as the most likely source of atmospheric Na^+. For the calculations of EF_{aer} and EF_{fog}, we used the median value of all $CCHO_{bulk} / Na^+_{bulk}$ ratios found in the samples of a certain sea-ice-related sea surface compartment (ice-free, leads and polynyas, MIZ, melt ponds) over the whole campaign.

$$EF_{SML} = \frac{[x]_{SML}}{[x]_{bulk}} \quad (1)$$

$$EF_{aer,stage\ y} = \frac{[x]_{aer,stage\ y}/[Na^+]_{aer,stage\ y}}{[x]_{bulk}/[Na^+]_{bulk}} \quad (2)$$

$$EF_{fog} = \frac{[x]_{fog}/[Na^+]_{fog}}{[x]_{bulk}/[Na^+]_{bulk}} \quad (3)$$

3 Results and discussion

The sources of SSA particles, and hence of atmospheric marine carbohydrates, microbial cells and fragments, in the Arctic are diverse and influenced by the prevailing sea ice conditions. Here, we present the concentrations and relative compositions of CCHO in the SML and bulk water from the ice-free ocean, open leads and polynyas within the pack ice, melt ponds and the MIZ. After this, the different sea-ice-related sea surface compartments are linked with the atmospheric CCHO found in ambient size-resolved aerosol particles and fog water. The influences of the air mass history, enrichments of CCHO towards Na^+ during the sea–air transfer and secondary atmospheric transformations processes altering atmospheric CCHO are discussed.

3.1 Sea ice influences the properties of the sea surface water

Variable CCHO concentrations in the Arctic surface water. CCHO was found in the dissolved (*d*CCHO) and particulate (*p*CCHO) phases of the SML and bulk water samples collected from the ocean and the melt ponds during the PS106 campaign. Among all aqueous samples, regardless of the sampling environment and depth (SML versus bulk), *d*CCHO (13–640 $\mu g\,L^{-1}$; $mean_{dCCHO} = 82 \pm 110\,\mu g\,L^{-1}$; $n = 70$) and *p*CCHO (4–810 $\mu g\,L^{-1}$; $mean_{pCCHO} = 84 \pm 160\,\mu g\,L^{-1}$; $n = 70$) concentrations were highly variable. However, the minimum, maximum and mean values of both *d*CCHO and *p*CCHO ranged within the same orders of magnitude. CCHO as the sum of *d*CCHO and *p*CCHO ranged between 22–1070 $\mu g\,L^{-1}$ ($mean_{CCHO} = 166 \pm 250\,\mu g\,L^{-1}$; $n = 70$).

Large differences in the mean values and standard deviations of CCHO were observed among the four sea-ice-related sea surface compartments in the Arctic (leads and polynyas within the pack ice, MIZ, ice-free ocean, melt ponds) as shown in Fig. 2a and b. The highest mean values for *d*CCHO and *p*CCHO were observed in the SML of the MIZ ($mean_{dCCHO,SML,MIZ} = 190 \pm 160\,\mu g\,L^{-1}$; $mean_{pCCHO,SML,MIZ} = 370 \pm 310\,\mu g\,L^{-1}$; $n = 5$) and melt ponds ($mean_{dCCHO,SML,melt\ ponds} = 190 \pm 240\,\mu g\,L^{-1}$; $mean_{pCCHO,SML,melt\ ponds} = 200 \pm 310\,\mu g\,L^{-1}$; $n = 6$), while the SML of the lead and polynya ($mean_{dCCHO,SML,leadandpolynya} = 70 \pm 75\,\mu g\,L^{-1}$; $mean_{pCCHO,SML,leadandpolynya} = 70 \pm 120\,\mu g\,L^{-1}$; $n = 20$) and ice-free open ocean ($mean_{dCCHO,SML,ice\text{-}free} = 73 \pm 12\,\mu g\,L^{-1}$; $mean_{pCCHO,SML,ice\text{-}free} = 36 \pm 5\,\mu g\,L^{-1}$; $n = 4$) samples tended to contain less CCHO. CCHO concentrations exhibited significant variability among the melt ponds, with higher concentrations observed in aged ponds (depths ranging from 40 cm to open-bottomed) compared to younger ones, where depths varied between 20 and 40 cm.

The lower SML concentrations from this study for the Arctic ice-free open ocean and lead and polynya samples align closely with several other investigations. Specifically, our results are comparable to Gao et al. (2012), who studied the SML of Arctic leads ($mean_{dCCHO,SML,Arctic\ leads} = 163 \pm 104\,\mu g\,L^{-1}$; $mean_{pCCHO,SML,Arctic\ leads} = 35 \pm 25\,\mu g\,L^{-1}$; $n = 4$), and Zeppenfeld et al. (2021), focusing on the ice-free part of the Southern Ocean west of the Antarctic Peninsula during the austral summer ($mean_{dCCHO,SML,Southern\ Ocean} = 48 \pm 63\,\mu g\,L^{-1}$; $mean_{pCCHO,SML,Southern\ Ocean} = 72 \pm 53\,\mu g\,L^{-1}$; n=18). Similarly, our data mirror findings from the tropical Cabo Verde ($mean_{dCCHO,SML,Cabo\ Verde} = 85 \pm 30\,\mu g\,L^{-1}$; van Pinxteren et al., 2023) and the Peruvian upwelling region ($mean_{dCCHO,SML,Peru} \approx 92 \pm 32\,\mu g\,L^{-1}$; Zäncker et al., 2017). Consequently, the Arctic MIZ and melt ponds, especially the aged ones with advanced microbiological activities, stood out with elevated CCHO within the Arctic and also compared to tropical and other polar regions.

Variable enrichments of CCHO in the SML. The enrichment factors (EF_{SML}) of the CCHO in the SML relative to the corresponding bulk water ranged between 0.4 and 16 for *d*CCHO (Fig. 2c), while the EF_{SML} for *p*CCHO varied between 0.4 and 49 (Fig. 2d); 80 % of the SML samples were moderately or highly enriched in marine carbohydrates with only a few cases of depletion (7 for *d*CCHO and 8 for *p*CCHO out of 35 in total). With a median $EF_{SML,pCCHO,MIZ}$ value of 3.8 and a mean of 13.8, the enrichment of *p*CCHO in the MIZ stood out compared to the *p*CCHO in other sea-ice-related sea surface compartments and to *d*CCHO overall. However, it should be noted that the number of MIZ samples was low, and median and mean values were dominated by three sample pairs with very high EF_{SML} values. Low to moderate enrichments for *d*CCHO and *p*CCHO were typically found in the lead and polynya samples from the pack ice (median $EF_{SML,dCCHO,leadsandpolynyas} = 1.9$; median $EF_{SML,pCCHO,leadsandpolynyas} = 2.0$, $n = 20$). However, three

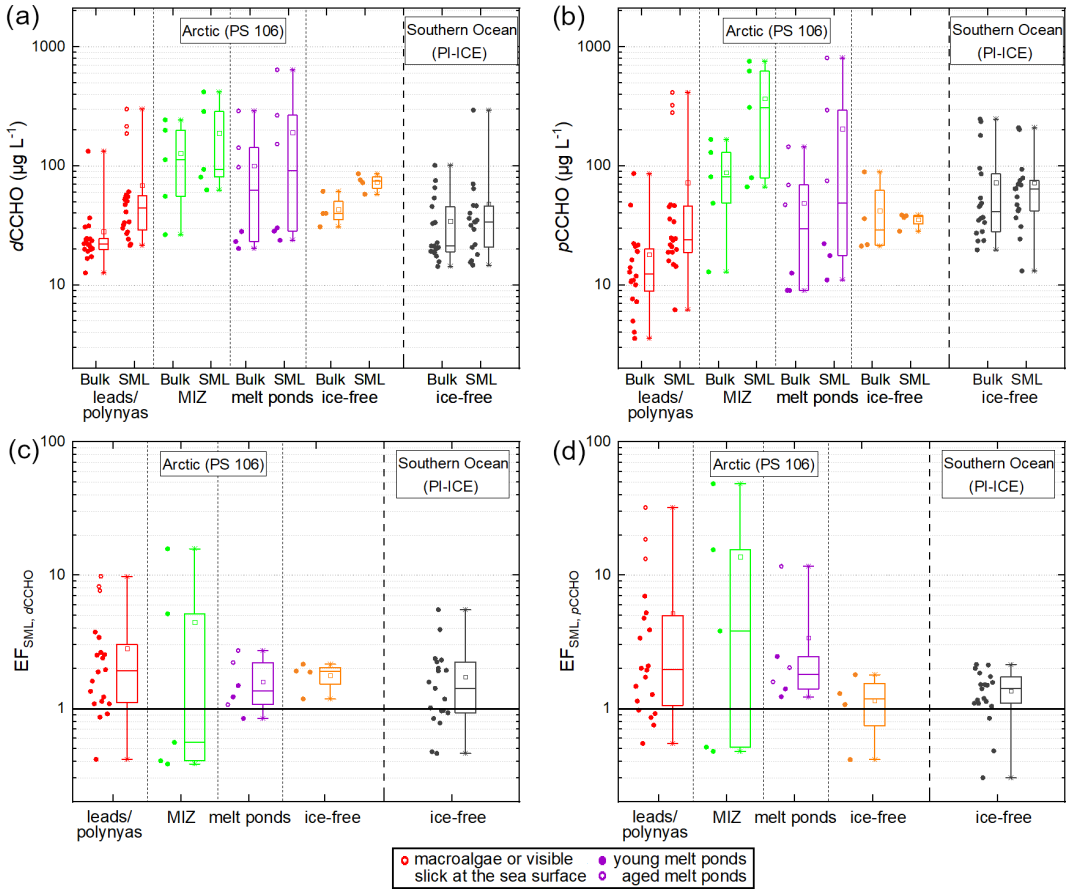

Figure 2. Scattered box-and-whisker plots showing the concentrations of **(a)** *d*CCHO and **(b)** *p*CCHO in the bulk and SML samples from the open leads and polynyas in the pack ice (red), the MIZ (green), ice-free open ocean (orange) and young and aged melt ponds (purple) collected during the PS106 campaign in the Arctic in comparison to the ice-free part of the Southern Ocean west of the Antarctic Peninsula investigated during the PI-ICE campaign in 2019 (black) as published in Zeppenfeld et al. (2021a). EFs between SML and bulk water are shown in **(c)** for *d*CCHO and **(d)** for *p*CCHO. The black horizontal line represents an EF = 1, meaning no enrichment or depletion.

lead samples showed quite high *d*CCHO and *p*CCHO concentrations in the SML compared to the corresponding bulk samples resulting in high $EF_{SML,dCCHO,leadsandpolynyas}$ up to 10 and $EF_{SML,pCCHO,leadsandpolynyas}$ up to 32. The exceptionally high EFs of these three samples can be explained by the observation of slicks – visible films on the sea surface with altered reflectance and typically high enrichments of organics (Cunliffe et al., 2013; Stolle et al., 2010; Williams et al., 1986; Wurl et al., 2009) as well as the presence of macroalgae floating at the ocean's surface near the sampling site. Even though the macroalgae were not collected themselves, their exudates or fragments might have been released, accumulated and distributed in the SML close-by and thus sampled. Consequently, the few samples with high EFs in open leads might rather represent exceptional events as spatially small-scale phenomena.

The slight to high enrichments for *d*CCHO and *p*CCHO in this study are in good agreement with the values reported by Gao et al. (2012), who determined $EF_{SML,dCCHO}$ between 3.5 and 12 and $EF_{SML,pCCHO}$ between 1.7 and 7.0 for open leads within the central Arctic Ocean. Furthermore, the $EF_{SML,dCCHO}$ of the four Arctic sea-ice-related sea surface compartments reported here were not significantly different compared to values found in the ice-free part of the Southern Ocean (ANOVA, one-way, 0.05 significance level). For the *p*CCHO, however, the average EF_{SML} in the Arctic MIZ was significantly higher than the one of the Southern Ocean, whereas the $EF_{SML,pCCHO}$ of the ice-free ocean in the Arctic was similar to the Southern Ocean.

For explaining the accumulation in the SML, previous studies proposed several mechanisms and processes, which fundamentally differ for the dissolved and particulate carbohydrates. The enrichment of *p*CCHO in the SML might be dominated by an interplay of density-related and wind-driven processes. For instance, the positive buoyancy of TEP, a subgroup of *p*CCHO, leads to an upward flux serving as a continual vehicle for marine organisms and attached chemical compounds (Azetsu-Scott and Passow, 2004; Mari

et al., 2017). Furthermore, strong winds can cause a short-term mixing of the upper water column reducing the EF_{SML} of particulates (Obernosterer et al., 2008) or TEP (Wurl et al., 2009; Zäncker et al., 2021), while the wind-induced entrainment of air and the bubbling of seawater convert dissolved negatively charged *d*CCHO and colloids into larger aggregates due to their sticky properties leading to an enrichment of *p*CCHO in the SML (Passow, 2002; Robinson et al., 2019; Wurl et al., 2011). The enrichment of *d*CCHO and also *d*FCHO in the SML is attributed to co-adsorption to other surface-active compounds from the seawater matrix being scavenged at the surface of rising bubbles (Burrows et al., 2016; Hasenecz et al., 2020; Schill et al., 2018; Xu et al., 2023). Additionally, microbial processes in the SML could enhance the enrichment through in situ *d*CCHO production by micro- or macroalgae, while photolysis and enzymatic degradation of *d*CCHO into *d*FCHO by heterotrophic bacteria could decrease the SML enrichment. Specific to the Arctic, the release of meltwater from the sea ice could be an additional source for carbohydrates in the SML, considering the production of CCHO, exopolymeric substances (EPSs) and TEP by sea ice algae and bacteria as a protection strategy against freezing damage and fluctuating salinity in sea ice (Aslam et al., 2016; Krembs et al., 2002; Krembs and Deming, 2008). This aligns well with the finding by Galgani et al. (2016), who observed labile, fresh OM in the SML of melt ponds compared to the rather old, refractory nature of the SML in the surrounding open leads. Hence, melting of sea ice could explain the extraordinarily high EF_{SML} observed in some, but not all, SML samples from the MIZ and melt ponds. In summary, several processes might be responsible for enrichment processes in the SML, especially in the Arctic, where the melting of sea ice could strongly bias the physiochemical processes usually observed in controlled tank experiments.

High and low salinities due to freezing and melting of sea ice. While the surface seawater of the Arctic Ocean is very saline, the Arctic sea ice is much fresher due the separation into salt-free ice crystals and a salty brine during its formation from seawater and a subsequent salt loss from gravity drainage in winter and flushing during summer (Notz and Worster, 2009). During the late spring and summer period of this study, when strong melting of sea ice occurs, a large amount of freshwater enters the surface of the ocean creating inhomogeneities of salinity within the surface of the ocean. In both the ice-free ocean and the pack ice, where sea ice exists, but the melting rate is low, salinities of the SML and the bulk water ranged in this study between 30.9 and 34.5 (Zeppenfeld et al., 2019b), which is typical for the SML and the surface bulk water of the Arctic Ocean (Vaqué et al., 2021). Within the MIZ, where freshwater from melting sea ice quickly mixes with the salty ocean water, salinities were similar with values in this study between 30.1 and 33.4, however, also with an exception in the SML of 25.7. Melt ponds that were not yet joined at the bottom with the ocean below were much fresher with lower and more variable salinities ranging from 4.3 to 19.5 (Zeppenfeld et al., 2019b). With a few exceptions, salinity discrepancies between the SML and the corresponding bulk water were small in most cases.

Sea–air transfer studies usually refer to open-ocean scenarios with high salinities in the seawater and without the presence of melting sea ice. For the calculation of enrichment factors of organics in aerosol particles (EF_{aer}) or fog (EF_{fog}), the concentration of Na^+ – a major compound of sea salt – in the seawater bulk is included by default (see Eqs. 2 and 3). However, the Arctic is a more complex marine environment where salinities, and hence Na^+ concentrations, can vary widely as melting progresses. This may strongly influence the mechanisms behind the bubble bursting process, the $CCHO / Na^+$ ratios in the bulk seawater and the SML, and thus also the EF_{aer} and EF_{fog} as it will be discussed in Sect. 3.4. Consequently, the variability of salinity in Arctic seawater and melt ponds should be considered for sea–air transfer studies that rely on Na^+ values.

Four sea-ice-related sea surface compartments with different characteristics. The high Arctic differs from other oceanic regions in the presence, formation and melting of sea ice creating sea-ice-related sea surface compartments (ice-free, leads and polynyas, MIZ, melt ponds) with individual biological and chemical characteristics, such as CCHO concentrations, enrichments in the SML and salinities. This might potentially impact the transfer of substances from the ocean to the atmosphere, chemo-selective enrichment processes of marine CCHO in the primary marine aerosol particles and thus their microphysical properties. The next sections will elucidate if and how these differences within the individual compartments relate to $CCHO_{aer}$ and $CCHO_{fog}$.

3.2 Sea spray aerosol and therein contained combined carbohydrates

Breaking waves as the main mechanism for SSA emissions is not unambiguous in the Arctic. In the open ocean, the emission flux of SSA and hence its inorganic and organic constituents mainly depend on the wind speed as the driving force for breaking waves and bubble bursting, and furthermore on the seawater temperature, salinity, wave properties and organic surface-active substances (Grythe et al., 2014). In this study, atmospheric sodium ($Na^+_{aer,PM_{10}}$), the best tracer for SSA (Barthel et al., 2019), ranged between 12 and 765 ng m^{-3} (Table S1). $Na^+_{aer,PM_{10}}$ showed a good correlation ($R = 0.80$, $p < 0.001$, Fig. 3a) with wind speed, measured at the sampling site and averaged over the sampling time, if all aerosol samples are included. However, the strength of this correlation decreased sharply ($R = 0.59$, $p < 0.1$), when only samples collected over the MIZ and the pack ice were included, while the few samples from the open ocean characterized by high Na^+ values were excluded. This is due to the presence of sea ice in the high Arctic, which likely alters and conceals the classical wind-driven mech-

anisms of breaking waves and bubble bursting resulting in SSA emission. Firstly, sea ice covers a significant part of the Arctic Ocean strongly reducing the area releasing SSA. Secondly, the presence of sea ice causes an attenuation of the high-frequency wind–sea waves, while longer waves, such as swells, can remain (Thomson, 2022). Consequently, the effect of wind on the SSA emission mechanisms within the open leads and the MIZ might be different than in the ice-free ocean. For those sea-ice-dominated compartments, alternative wind-independent sources of ascending bubbles were suggested, such as melting sea ice nearby, respiration of phytoplankton or sea–air heat exchange below the sea surface (Chen et al., 2022, and references therein). Thirdly, in contrast to other marine regions with quite homogeneous ocean salinities, and hence sodium concentrations, the salinities among the different Arctic sea-ice-related sea surface compartments are more variable due to the melting of sea ice. Previously, the results of a sea–air transfer tank experiment with artificial seawater showed the influence of salinity on the relative particle number concentrations of emitted SSA for salinities below 15 – values especially relevant for melt ponds in the Arctic – while changes at higher salinities did not result in a measurable effect (Zábori et al., 2012). Additionally, organics with potential surface-active properties are very variable in these disparate Arctic environments, as discussed for CCHO in Sect. 3.1. Organic surfactants can alter the ocean surface's ability to form whitecaps and the lifetime of bubbles (Bigg and Leck, 2008; Callaghan et al., 2012; Grythe et al., 2014) and therefore SSA properties.

Finally, blowing snow over the sea ice could serve as an additional source of atmospheric Na^+_{aer} when a certain air-temperature-dependent wind speed threshold is exceeded (Chen et al., 2022; Gong et al., 2023; Huang and Jaeglé, 2017; Yang et al., 2008). Consequently, connections and correlations for the release of SSA particles in the heterogeneous high Arctic are more difficult to explore than other marine environments without sea ice. It can be assumed that this complex setting influences not only the release of inorganic constituents from seawater, but also its organic compounds, such as CCHO.

$CCHO_{aer}$ distributed in all size modes. During the PS106 campaign, the overall atmospheric concentrations of $CCHO_{aer,PM_{10}}$ ranged between 0.5 and 4.7 ng m^{-3} (Table S1). Combined carbohydrates were found on both supermicron ($CCHO_{aer,super} = 0.07$–2.1 ng m^{-3}) and submicron particles ($CCHO_{aer,sub} = 0.26$–4.4 ng m^{-3}). Thus, these $CCHO_{aer}$ values ranged within the same orders of magnitude as in the Arctic studies by Karl et al. (2019) and Leck et al. (2013) or the study conducted at the western Antarctic Peninsula by Zeppenfeld et al. (2021a). $CCHO_{aer}$ appeared in all of the five size classes in variable concentrations (Fig. 4a). Although the average concentrations were similar on all stages, local maxima were observed on stages 2 (0.14–0.42 µm) and 5 (1.2–10 µm). A similar size distribution of marine $CCHO_{aer}$ in these specific size ranges, but more pronounced, has been already observed in the ice-free part of the Southern Ocean by Zeppenfeld et al. (2021a) explaining these findings with a likely release of marine polysaccharides from the ocean as part of film and jet droplets. Possibly, the aerosol size distribution of marine polysaccharides resulting from wind-driven bubble bursting emissions is not as obvious in this Arctic study as it was in the ice-free Southern Ocean due to the presence of Arctic sea ice suppressing and altering the local SSA emission mechanisms as indicated in

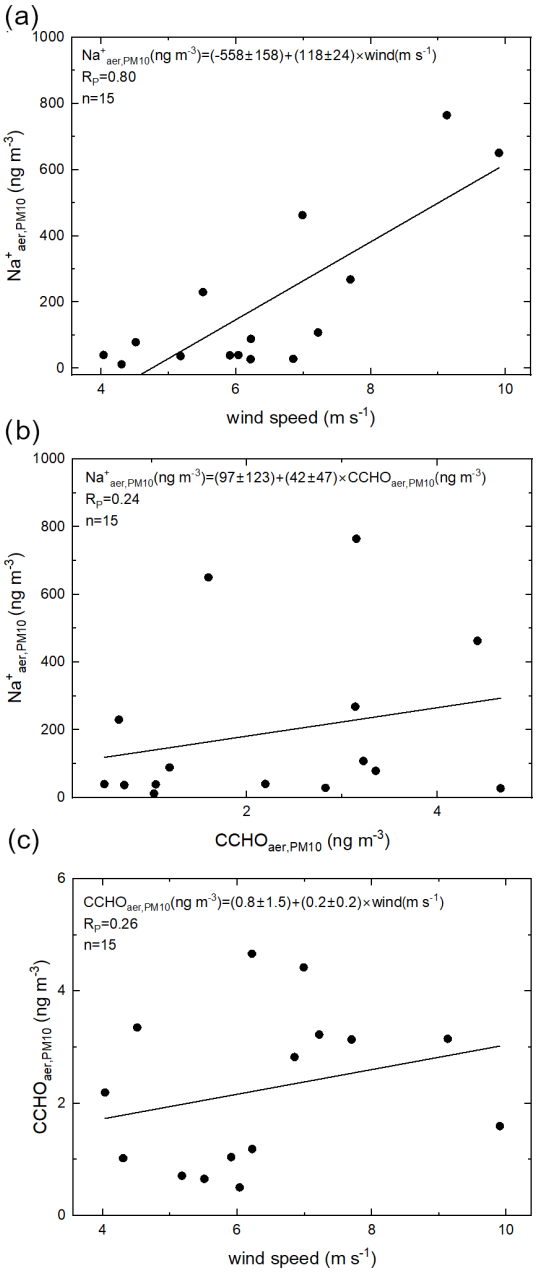

Figure 3. Correlations between **(a)** $Na^+_{aer,PM_{10}}$ and the averaged wind speed, **(b)** $Na^+_{aer,PM_{10}}$ and $CCHO_{aer,PM_{10}}$, and **(c)** $CCHO_{aer,PM_{10}}$ and averaged wind speed.

the previous section. The relative contribution of $CCHO_{aer}$ to $mass_{aer}$ varied between 0.01 % and 4 % (Fig. 4b), while the carbon contained within the combined carbohydrates (C–$CCHO_{aer}$) contributed 0.06 % to 4.9 % to the OC_{aer} in the size-resolved aerosol particles (Fig. 4c). These contributions agree well with the findings in marine aerosol particles from the Southern Ocean (Zeppenfeld et al., 2021a).

Unlike the study conducted in the Southern Ocean (Zeppenfeld et al., 2021a), $CCHO_{aer,PM_{10}}$ in this study showed no significant correlations with $Na^{+}_{aer,PM_{10}}$ ($R = 0.24$, $p > 0.1$, Fig. 3b) or wind speed ($R = 0.26$, $p > 0.1$, Fig. 3c). The presence of sea ice resulting in melt ponds and MIZ regions and the interplay of multiple emission mechanisms in the Arctic, as discussed earlier, could account for this complexity. However, if the correlations are resolved for the different Berner impactor stages (i.e., size ranges), a large variability can be observed (Fig. 5). A higher correlation was found especially in stage 4 (1.2–3.5 µm) between $CCHO_{aer,stage\ 4}$ and $Na^{+}_{aer,stage\ 4}$ ($R = 0.76$, $p < 0.01$), while the Pearson correlations coefficients for the other Berner stages were much lower. This could indicate the same marine source and wind-driven emission mechanism for both chemical constituents in this supermicron aerosol size mode, while other aerosol size modes might have been influenced by atmospheric aging and wind-independent emission mechanisms as already mentioned for Na^{+}_{aer} in the previous section. This observation agrees well with the findings by Bigg and Leck (2008) and Leck et al. (2002) reporting submicron polymer gel particles, likely consisting of polysaccharides, in the atmosphere of the high Arctic containing almost no sea salt and showing large similarities to those particles found in open leads closeby. This is quite surprising considering that the mechanism of wind-driven wave breaking is quite limited due to the lack of long fetches of open water (Held et al., 2011; Norris et al., 2011).

Blowing snow has been discussed as a possible additional source for atmospheric Na^{+}, raising the question of whether it could be a source of atmospheric carbohydrates, too. During this study, the measurements of *d*FCHO and CCHO in five Arctic snow samples collected resulted in low values mostly below the limits of detection. This finding supports the conclusion that blowing snow does not serve as a competitive source for the emission of atmospheric marine carbohydrates.

3.3 Marine combined carbohydrates in fog

The concentrations of $Na^{+}_{fog,liquid}$ (1.7–903 $mg\,L^{-1}$; mean $= 130 \pm 220\,mg\,L^{-1}$; $n = 22$) and $CCHO_{fog,liquid}$ (18–22 000 $\mu g\,L^{-1}$; mean $= 1380 \pm 4600\,\mu g\,L^{-1}$; $n = 22$) were very variable in fog water (Table S2). Atmospheric concentrations of these chemical constituents in fog droplets (indicated by the index "fog,atmos") can be calculated under consideration of the liquid water content (LWC) during the fog events. Since LWC was not measured during PS106 directly, the LWC was approximated from the measured CCN concentrations at the lowest quality-assured supersaturation of 0.15 % and an assumed average droplet diameter of 17 µm. This approach resulted in LWCs of $0.62 \pm 0.39\,g\,m^{-3}$ for the fog collected over the North Sea and Norwegian Sea and $0.10 \pm 0.09\,g\,m^{-3}$ for the fog over the Arctic Ocean (Hartmann et al., 2021). Following this approach, atmospheric concentrations in fog ranged between 0.12 and 150 $\mu g\,m^{-3}$ (mean $= 25 \pm 43\,\mu g\,m^{-3}$; $n = 16$) for $Na^{+}_{fog,atmos}$ and between 3 and 4300 $ng\,m^{-3}$ (mean $= 390 \pm 1100\,ng\,m^{-3}$; $n = 16$) for $CCHO_{fog,atmos}$, respectively. These atmospheric concentrations in fog are for both $Na^{+}_{fog,atmos}$ and $CCHO_{fog,atmos}$ by 1–3 orders of magnitude higher than the atmospheric concentrations in aerosols discussed in Sect. 3.2. This divergence may be explained by the following:

- Fog scavenging is a transfer process of aerosol particles into the liquid phase of fog droplets (Gilardoni et al., 2014). As fog forms and grows, it can capture aerosol particles in the air and increase their concentration within the fog droplets. This could lead to higher atmospheric concentrations of aerosol particle compounds, especially for the water-soluble and hygroscopic ones, inside the fog compared to the surrounding air.

- The activation of aerosol particles to fog droplets is a process dominated by particle size with larger particles tending to activate first. It is conceivable that SSA particles larger than 10 µm, usually few in number, but with a large mass contribution, were available near the sea surface, where sampling occurred. These SSA particles were activated into fog droplets and contributed significantly to the Na^{+} and CCHO in the fog. In contrast, aerosol sampling was restricted by the Berner impactor's 10 µm diameter cut-off neglecting the larger particles in the consideration.

- The LWC values were not measured but estimated, which could be a source of errors. This approach resulted in values representing rather the upper limit of LWC values typically reported for Arctic summer fog (0.001–0.17 $g\,m^{-3}$ (Kumai, 1973)) or sea fog (0.02–0.1 $g\,m^{-3}$ (Herrmann et al., 2015)) but appear within a realistic range. Consequently, they are likely not responsible for the large difference between aerosol and fog concentrations of several orders of magnitude.

Since both organic and inorganic constituents showed higher atmospheric concentrations in fog/clouds compared to ambient aerosol particles, we conclude that a physical phenomenon, such as fog scavenging, might explain this observation and not an in situ formation within the cloud droplets. Similar to the findings of this study discussing marine CCHO and Na^{+} in Arctic fog, Triesch et al. (2021a) found strikingly

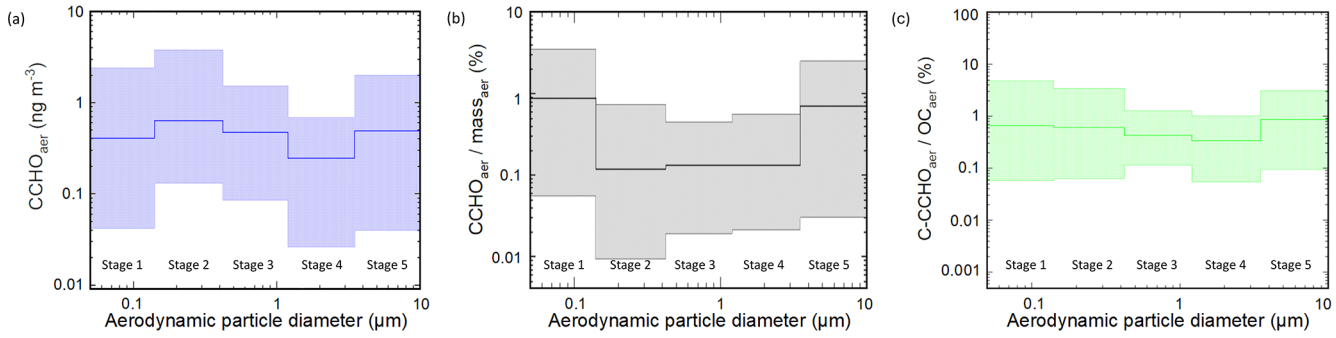

Figure 4. **(a)** Concentration of combined carbohydrates in size-resolved aerosol particles ($CCHO_{aer}$), **(b)** ratio of $CCHO_{aer}$ to the total particle mass concentration ($mass_{aer}$) and **(c)** ratios of carbon contained within the combined carbohydrates in aerosol particles ($C–CCHO_{aer}$) to organic carbon in aerosol particles (OC_{aer}). The bold lines represent the average concentrations during the PS106 campaign. The hatched areas show the range between the maximum and minimum values. The aerodynamic particle diameter refers to sampling conditions at relative humidity of max. 80 %.

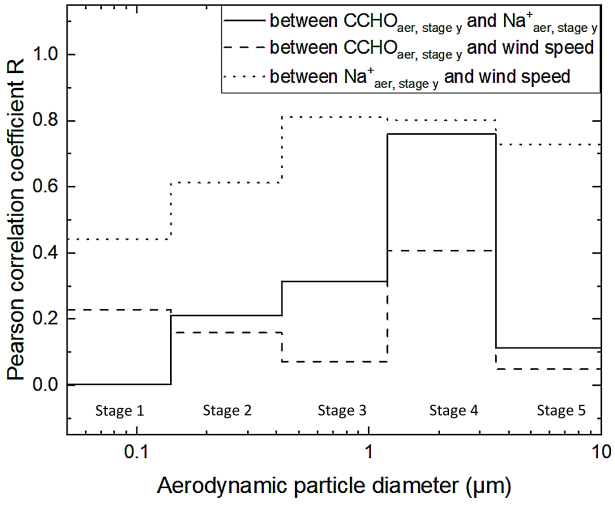

Figure 5. Pearson correlation coefficient R between $CCHO_{aer,stage\ y}$ and $Na^+_{aer,stage\ y}$ (solid line), between $CCHO_{aer,stage\ y}$ and the average wind speed (dashed line), and between $Na^+_{aer,stage\ y}$ and the average wind speed (dotted line) for each stage y of the Berner impactor.

high concentrations of free amino acids (FAAs) and Na^+ in marine clouds compared to aerosol particles both collected on top of the Monte Verde on Cabo Verde as shown in Table 1.

While $dFCHO_{fog}$ and derivatives, such as anhydrosugars and sugar alcohols, have been readily reported for fog water with terrestrial and marine background (Dominutti et al., 2022), we here present for the first time ambient CCHO concentrations in marine fog.

3.4 Chemo-selective sea–air transfer of marine carbohydrates

The chemo-selective sea–air transfer of organics towards inorganic sea salt constituents has been described both in tank and ambient field studies for organic carbon in general (Gantt et al., 2011; Hoffman and Duce, 1976; van Pinxteren et al., 2017) or several chemical constituents, such as carbohydrates (Hasenecz et al., 2020; Schill et al., 2018; Zeppenfeld et al., 2021a), lipids (Triesch et al., 2021b) and free and combined amino acids (Triesch et al., 2021a, c).The calculation of dimensionless ratios between the concentrations of the examined organic parameter and Na^+ allows a comparison of aquatic and atmospheric samples within the marine environment. Figure 6 shows the CCHO / Na^+ ratios for the bulk and SML in the four sea-ice-related sea surface compartments, size-resolved aerosol particles and fog water collected during the PS106 cruise.

Wide range of CCHO / Na^+ ratios in Arctic surface seawater. In the surface seawater samples of this study, the CCHO / Na^+ ratios spanned from 2×10^{-6} to 8×10^{-4}, representing a wider range than those found in the Southern Ocean (9×10^{-7} and 3×10^{-5}; Zeppenfeld et al., 2021a). While the ratios in the SML and bulk water in general ranged in the same orders of magnitude, large differences were observed in the individual Arctic sea-ice-related sea surface compartments. In the SML, the lowest median values were found in the leads and polynyas and ice-free ocean samples with 6×10^{-6} and 9×10^{-6}, respectively, while higher median values appeared in the SML of the MIZ (3×10^{-5}) and melt ponds (4×10^{-5}), or even 6×10^{-4}, when only aged melt ponds were considered. This large variability of CCHO / Na^+ ratios can be explained by the variable content of CCHO (high CCHO content in aged melt ponds and MIZ versus lower CCHO content in ice-free ocean and leads and polynyas) and Na^+ (low salinity in the SML of melt ponds versus higher salinities in ice-free ocean and

Table 1. Atmospheric concentrations of selected SSA constituents in fog or clouds compared to ambient aerosol particles during marine field studies.

Chemical constituent	Fog/cloud ($ng\,m^{-3}$)	PM_{10} ($ng\,m^{-3}$)	Sampling location	Sampling height (m a.s.l.)[h]	Sampling period	Reference
*d*FCHO	9.2–52[a,b]	–	Reúnion	1760[d]	Mar–Apr 2019	Dominutti et al. (2022)
	1.5–1040 (mean: 80 ± 260)	< LOD-2.0	Arctic	25[e]	May–Jul 2017	this study
CCHO	3–4300 (mean: 390 ± 1100)	0.5–4.7	Arctic	25[e]	May–Jul 2017	this study
FAA	11–490	1.0–4.8	Cabo Verde	744[f]	Sep–Oct 2017	Triesch et al. (2021a)
	6–79[b]	–	Reúnion	1760[d]	Mar–Apr 2019	Dominutti et al. (2022)
	($\mu g\,m^{-3}$)	($\mu g\,m^{-3}$)		(m a.s.l.)[h]		
Na^+	1.6–7.2	0.17–0.40	Cabo Verde	744[f]	Sep–Oct 2017	Triesch et al. (2021a)
	0.1–2.2[b]	–	Reúnion	1760[d]	Mar–Apr 2019	Dominutti et al. (2022)
	0.014–0.063[c]	–	Arctic	180–374[g]	Aug–Sep 2018	Zinke et al. (2021)
	0.12–150 (mean: 25 ± 43)	0.012–0.77	Arctic	25 m[e]	May–Jul 2017	this study

[a] Only includes free glucose and rhamnose; sugar alcohols and anhydrosugars were not included for this table. [b] Values were calculated from LWCs, molecular weights and concentrations in fog water given within the reference; terrestrial contributions are likely. [c] Calculated from concentration in fog water and an assumed LWC of $0.1\,g\,m^{-3}$. [d] Piste Omega. [e] RV *Polarstern*. [f] Monte Verde. [g] Tethered balloon, [h] "m a.s.l" denotes "meters above sea level".

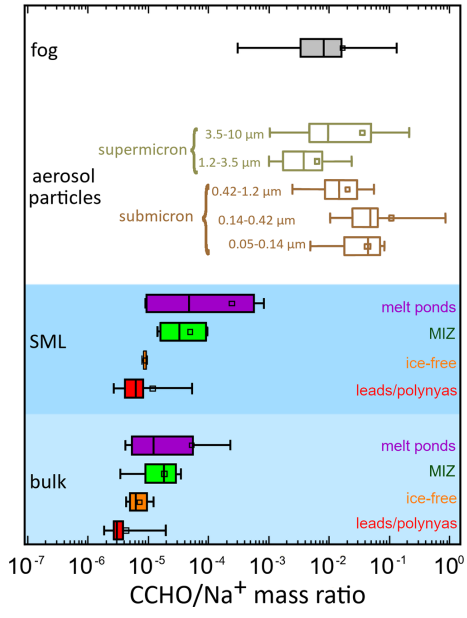

Figure 6. CCHO / Na^+ ratios for CCHO in Arctic fog, size-resolved aerosol particles and the surface seawater (SML and bulk) from melt ponds, the marginal ice zone (MIZ), the ice-free ocean and leads and polynyas from the pack ice.

leads and polynyas and MIZ) in the different sea-ice-related sea surface compartments. It can be expected that the different CCHO / Na^+ ratios in the individual seawater compartments impacted the corresponding CCHO / Na^+ ratios in fog and aerosol particles during the sea–air transfer and consequently the enrichment factors for the sea–air transfer (EF_{aer}, EF_{fog}), which are calculated from those ratios.

Air mass history influences $CCHO_{aer}$ / Na^+_{aer} ratios in Arctic aerosol particles. In contrast to the seawater samples, $CCHO_{aer}$ / Na^+_{aer} ratios were much higher for aerosol particles considering the size resolution (1×10^{-3}–9×10^{-1}) supporting the concept of the chemo-selective enrichment of carbohydrates towards Na^+ during the transfer from the ocean into the atmosphere. In this context, submicron particles showed much higher median ratios of 4×10^{-2} (0.05–0.14 µm) and 4×10^{-2} (0.14–0.42 µm) than supermicron particles with 4×10^{-3} (1.2–3.5 µm) and 1×10^{-2} (3.5–10 µm). Regarding PM_{10} (sum of all five Berner stages), the $CCHO_{aer,PM_{10}}$ / $Na^+_{aer,PM_{10}}$ ratios varied much more in the Arctic study presented here (2×10^{-3}–2×10^{-1}, see Table S1) than in the ice-free part of the Southern Ocean (8×10^{-4}–7×10^{-3}; Zeppenfeld et al. (2021b)).

During four aerosol sampling periods (24–26 May 2017; 26–29 May 2017; 29 May–1 June 2017; 19–25 June 2017), air masses had predominantly passed over the ice-free ocean (45 %–100 % of the 12 h prior to sampling, as shown in Table S1 and Fig. S2). Interestingly, these periods exhibited the lowest $CCHO_{aer,PM_{10}}$ / $Na^+_{aer,PM_{10}}$ ratios (2×10^{-3}–9×10^{-3}, detailed in Table S1), values that are strikingly similar to those observed in the ice-free Southern Ocean. In contrast, higher ratios were found, when the air masses had rested a significant time over the pack ice or the MIZ. This could be an indication that the chemical composition of

the sea-ice-related sea surface compartments, here the ice-free ocean with low CCHO / Na^+ ratios, strongly influences the relative composition of aerosol particles. In contrast, the influence of the MIZ, pack ice and melt ponds exhibiting quite different chemical, physical and biological properties on $CCHO_{aer,PM_{10}}$ / $Na^+_{aer,PM_{10}}$ could not be resolved in further details following this approach using back-trajectory calculations and satellite data. This is certainly due to the proximity of these sea-ice-related sea surface compartments on a small spatial scale (especially melt ponds in direct vicinity to open leads), the long sampling periods of aerosol particles, the lacking knowledge of deposition rates, the effect of wind on wave propagation and bubble bursting processes within the individual sea-ice-related sea surface compartments and missing data on the biological activities in individual melt ponds.

Similar CCHO / Na^+ ratios in aerosol particles and fog. For fog, $CCHO_{fog}$ / Na^+_{fog} ratios ranged from 3×10^{-4} to 1×10^{-1}, which covers the same orders of magnitude of aerosol particles. Even though absolute atmospheric concentrations of CCHO are much higher in fog than in aerosol particles possibly due to fog scavenging (as discussed in Sect. 3.3), the CCHO / Na^+ ratios were similar. This strongly implies that $CCHO_{fog}$ actually originated from the ambient marine aerosol particles. The attempt to find matches or common trends between aerosol particles and the fog in individual samples was not successful, certainly due to the very different resolutions of sampling times and in addition due to the probability of fog droplets containing aerosol particles bigger than 10 µm.

Calculated EF_{aer} and EF_{fog} depend on the sea-ice-related marine source under consideration. EF_{aer} and EF_{fog} are calculated as a quotient between the CCHO / Na^+ ratios in the size-resolved aerosol particles or fog, and the corresponding bulk water. The CCHO / Na^+ ratios in the Arctic seawater of this study were very variable depending on the regarded sea-ice-related sea surface compartment environment, as well in the aerosol particles and in fog water. This fact strongly impacted the resulting hypothetical EF_{aer} and EF_{fog}, enabling calculated values ranging between 10^1 and 10^4 for supermicron aerosol particles, between 10^2 and 10^5 for submicron particles and between 10^0 and 10^4 for fog depending on which sea-ice-related sea surface compartment was assumed as the marine source of SSA as shown in Fig. 7. Due to missing information, including SSA emission fluxes from the four sea-ice-related compartments, aerosol deposition rates, biological activities in melt ponds, wind effects on wave propagation and bubble bursting, and the comparative importance of melt ponds versus open leads (which are in close proximity, making it difficult to resolve them in back-trajectory analyses) as SSA sources – we did not perform calculations based on the back-trajectory history of each atmospheric sample. Instead, subsequent calculations for EF_{aer} and EF_{fog} employed a hypothetical approach, assessing the range of enrichment factors by considering only one of the four sea-ice-related compartments – represented by the corresponding median $CCHO_{bulk}$ / Na^+_{bulk} ratios – as the only source while excluding the others.

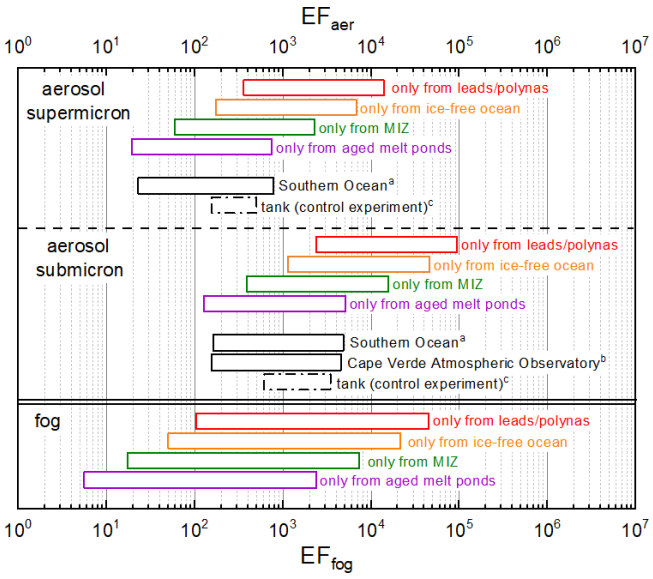

Figure 7. Range of calculated hypothetical enrichment factors EF_{aer} and EF_{fog} assuming either leads and polynyas, the ice-free ocean, the MIZ or aged melt ponds as the only marine source for the sea–air transfer of CCHO in the Arctic. For the calculation of EF_{aer} and EF_{fog}, the minimum and maximum values of the $CCHO_{aer/fog}$ / $Na^+_{aer/fog}$ ratios and the median values of $CCHO_{bulk}$ / Na^+_{bulk} were used. The EF_{aer} values of this study were compared with the results of **(a)** the field study conducted in the Southern Ocean by Zeppenfeld et al. (2021a), **(b)** the field study conducted at Cape Verde Atmospheric Observatory (CVAO) by van Pinxteren et al. (2023) and **(c)** the results of the CCHO tank study by Hasenecz et al. (2020) without any addition of heterotrophic bacteria (control experiment). Here, EF_{aer} values were calculated from the experimental data published by Hasenecz et al. (2020).

Lower atmospheric EFs were calculated when aged melt ponds ($EF_{aer,super}$ = 19–750; $EF_{aer,sub}$ = 127–5100; EF_{fog} = 5–2400), or the MIZ ($EF_{aer,super}$ = 60–2310; $EF_{aer,sub}$ = 390–16 000; EF_{fog} = 17–7400) were assumed as the only (theoretical) source of CCHO and Na^+, while higher values were found with the ice-free ocean ($EF_{aer,super}$ = 175–6800; $EF_{aer,sub}$ = 1100–46 000; EF_{fog} = 50–22 000) or open leads and polynyas ($EF_{aer,super}$ = 360–14 000; $EF_{aer,sub}$ = 2360–95 000; EF_{fog} = 103–44 600). It is important to note that EFs were most consistent with results from other CCHO sea–air transfer studies in the tank (Hasenecz et al., 2020) and the field (Zeppenfeld et al., 2021a), when aged melt ponds or the MIZ was considered as the only emission source. If leads and polynyas and the ice-free ocean were regarded as the only emission source, higher EF_{aer} and EF_{fog} values were obtained, and hence a possible overestimation of the mechanistic process of enrichment.

As the results on back-trajectory calculations and sea ice maps demonstrated (Table S1 and Fig. S2), most air masses were exposed to several of the sea-ice-related sea surface compartments before sampling. Consequently, none of the Arctic sea-ice-related sea surface compartments discussed above should be overlooked when discussing of sea–air transfer of organic substances.

During the same Arctic field campaign, Hartmann et al. (2021) investigated INP in ambient aerosol particles and compared it to bulk and SML in seawater from all the different sea-ice-related sea surface compartments using similar EF_{aer} calculations as reported here. They concluded that an enrichment of 3 to 5 orders of magnitude was necessary during the sea–air transfer to fully attribute atmospheric INP to oceanic sources. Here, we show that such high EF_{aer} and EF_{fog} for organics, and hence marine biogenic INP, can be calculated, e.g., when open leads and polynyas were referred to as the only oceanic source. In summary, Arctic air masses have been impacted by different types of sea-ice-related sea surface compartments before sampling, whereas it is still unclear which one has the biggest effect on the chemical composition of the marine aerosol particles. This aspect should be considered when the marine SSA constituents are modeled for the Arctic from remote sensing data.

3.5 Atmospheric aging of marine carbohydrates

To resolve the fate of marine carbohydrates in the atmosphere after their ejection from the ocean, the relative molar contributions of monosaccharides to CCHO were compared between the bulk and SML from the leads and polynyas, MIZ, ice-free ocean and melt pond samples, as well as the sub- and supermicron aerosol particles and fog water (Fig. 8). The composition of marine carbohydrates in seawater strongly depends on the dominating microbial species, season, diagenetic state, availability of nutrients and environmental stress factors (Engbrodt, 2001; Goldberg et al., 2011) leading to a natural variability among individual samples even within small spatial scales. Consequently, to enable the direct comparison of seawater with atmospheric samples of this field study with an elevated level of statistical certainty, here we compare the mean values of the entire data set, instead of individual samples. Finally, in addition to the changes of the monosaccharide patterns of CCHO, the systematic degradation of CCHO to *d*FCHO was observed in the atmosphere and will be discussed within this section.

CCHO composition in different sea-ice-related sea surface compartments and depths is similar. In seawater (bulk and SML), glucose (means = 35 mol %–48 mol %), galactose (means = 13 mol %–18 mol %) and xylose (means = 7 mol %–16 mol %) dominated the CCHO composition followed by smaller contributions of other neutral sugars, amino sugars, uronic acids and muramic acid (Fig. 8). Considering the natural variability among individual samples, there were no significant differences in means

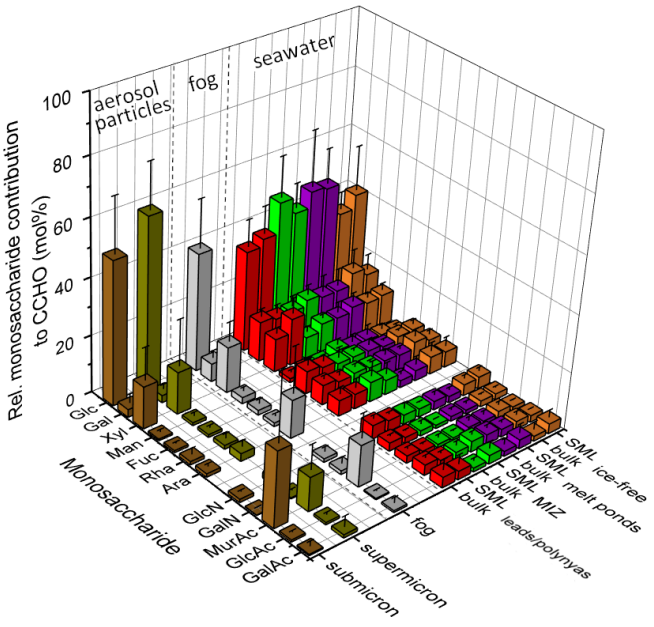

Figure 8. Relative monosaccharide composition of combined carbohydrates (CCHO) after acid hydrolysis in sub-/supermicron aerosol particles, fog water, bulk and SML samples from the leads and polynyas within the pack ice, the MIZ, the ice-free ocean, and young and aged melt ponds. The 3D bar chart shows the averages and standard deviations of the relative contributions. Glc: glucose, Gal: galactose, Xyl: xylose, Man: mannose, Fuc: fucose, Ara: arabinose, GlcN: glucosamine, GalN: galactosamine, MurAc: muramic acid, GlcAc: glucuronic acid, GalAc: galacturonic acid.

between the bulk and SML, nor among the lead and polynya, MIZ, ice-free ocean and melt pond samples. Variations were observed between the dissolved and particulate fractions (Fig. S3); nevertheless the combined carbohydrates within all sea-ice-related sea surface compartments followed the same pattern of the predominance of glucose, galactose and xylose. Overall, the relative monosaccharide compositions of glucose > (galactose ≈ xylose) > other (neutral or charged) monosaccharides of the seawater samples from this Arctic study appear similar to the monosaccharide compositions investigated in the SML and bulk water from the central Arctic Ocean (Gao et al., 2012) and at the western Antarctic Peninsula (Zeppenfeld et al., 2021a), the meltwater of Arctic multiyear sea ice (Amon et al., 2001) and the epipelagic water from the Ross Sea (Kirchman et al., 2001).

Less galactose but more muramic acid in atmospheric $CCHO_{aer}$ and $CCHO_{fog}$. Atmospheric samples showed a different monosaccharide pattern within the hydrolyzed CCHO in comparison to the seawater and melt pond samples. While glucose (means = 41 mol % for fog; 50 mol % for submicron and 60 mol % for supermicron aerosol particles) and xylose (means = 16 mol %, 15 mol % and 15 mol %) still prevailed over the relative monosaccharide pattern, the contribution of galactose (means = 6 mol %, 3 mol % and 3 mol %) was

strongly reduced, both in fog and aerosol particles. On the other hand, the ratio of muramic acid was strongly elevated in aerosol particles (means = 12 mol % and 26 mol %) and fog water (mean = 14 mol %) in comparison to the oceanic samples (means = 0.9 mol %–2.6 mol %). These differences of the relative monosaccharide contributions to CCHO among the seawater and the atmospheric samples described within this study are in good agreement with the sea–air transfer investigations conducted in the Southern Ocean at the western Antarctic Peninsula (Zeppenfeld et al., 2021a). Consequently, the occurring phenomenon might be independent of the sampling location and could be explained by three possible atmospheric processes, such as (1) a chemoselective sea–air transfer of certain oligo- or polysaccharides over others, (2) an atmospheric transformation due to abiotic chemical reactions or (3) an atmospheric transformation due to microbiological activities. Among these possible pathways, Zeppenfeld et al. (2021a) presumed the secondary atmospheric transformation caused by microbiological metabolism as the most probable or at least most dominant one supported by the prevalence of muramic acid, an amino sugar acid naturally occurring in bacterial cell walls (Mimura and Romano, 1985; Sud and Tyler, 1964), and the very selective absence of certain monosaccharides in the $CCHO_{aer}$ in aerosol particles as it was observed in this Arctic study as well.

Formation of combined arabinose in fog. A comparison of the monosaccharide composition of aerosol particles and fog water showed great similarity regarding dominant contributions from glucose, xylose and muramic acid. It seems plausible that the fog water droplets contained the same inorganic and organic compounds found in the SSA particles assuming that SSA particles activated the formation of fog droplets as CCN due to their rather large diameters and high hygroscopicity. Apart from that, however, a significant difference was observed in the increased relative contribution of arabinose in fog (mean = 13 mol %) compared to aerosol particles (means = 1.2 mol % and 2.7 mol %) indicating a formation of arabinose in the liquid phase. During a marine microcosm experiment performed by Hasenecz et al. (2020), a strong link was observed between the release of arabinose-containing polysaccharides in the form of EPSs and the presence of heterotrophic bacteria and stressed phytoplankton. Furthermore, a strain of the psychrotolerant marine bacterium *Pseudoalteromonas* sp. has been shown to produce EPSs mainly composed from glucose, arabinose and xylose (Casillo et al., 2018; Qin et al., 2007). Consequently, the release of arabinose-containing EPSs in fog could be a plausible protection mechanism of microorganisms contained within a droplet against freezing damage under low Arctic temperatures.

Indication for microbial activities in the atmosphere. Intact bacterial cells at atmospheric concentrations between 5×10^2 and 8×10^4 cells m^{-3} for remote marine and ice-covered regions (Šantl-Temkiv et al., 2018; Mayol et al., 2017), cell-bound and free enzymes have been detected in ambient and nascent marine super- and submicron aerosol particles during several field and tank studies (Aller et al., 2005; Hasenecz et al., 2020; Malfatti et al., 2019; Marks et al., 2001; Rastelli et al., 2017; Šantl-Temkiv et al., 2020; Uetake et al., 2020). To survive in this hostile environment, some of these microbes have developed a remarkable resilience to extreme environmental stressors, such as high UV radiation, radical exposure, changing osmolarity, freezing temperatures and desiccation. The selective enzymatic consumption of airborne labile carbohydrates explaining the loss of galactose and the persistence of xylose observed here could form a part of a survival strategy. Previous studies readily outlined additional adaptive strategies, including the release of protecting biofilms from EPSs, carotinoid pigmentation or the formation of own precipitating hydrometeors by enabling condensation on a surface as a CCN or freezing by IN active surfaces to reduce their atmospheric residence time (Delort et al., 2010; Matulová et al., 2014; Šantl-Temkiv et al., 2020). Consequently, an enzymatic transformation might serve as a plausible explanation for the selective removal of certain monosaccharides within $CCHO_{aer}$ and $CCHO_{fog}$ observed here. However, the survival and the metabolic activity of microorganisms is restricted by the presence of water (Ervens and Amato, 2020; Haddrell and Thomas, 2017) identifying liquid hydrometeors or fresh SSA as the most biologically active atmospheric hotspots. In contrast to most of the ambient aerosol particles, fog droplets provide enough water essential for bacterial activities. However, they might freeze under Arctic sub-zero temperatures possibly causing damage to the microbial cells, which might explain an in situ formation of a protecting biofilm from arabinose-containing EPSs. In a previous Arctic study, Orellana et al. (2011) readily detected microgels in aerosol particles, cloud and fog water most likely emitted from the surface water and the SML via bubble bursting. Indications for an in situ generation of marine microgels in fog water as an additional source to the primary release from the ocean by bubble bursting have been observed by van Pinxteren et al. (2022) in the tropical Atlantic Ocean.

The selective sea–air transfer of certain carbohydrates over others and the abiotic degradation as further possible pathways to the biotic transformation of marine $CCHO_{aer}$ have been discussed in detail in Zeppenfeld et al. (2021a) but do not appear, based on the current state of knowledge, as likely explanations of the very selective CCHO degradation and formation of other CCHO observed here. More future lab and mesocosm experiments are required to elucidate the contribution of each of these processes. Finally, the similarity between the carbohydrate compositions of fog water and aerosol particles, both two atmospheric compartments collected with different instrumentation, allows us to rule out artifacts of the different sampling and extraction techniques as a reason for the observed differences to the seawater.

Depolymerization of CCHO to dFCHO, seawater versus atmosphere. Free glucose, by far the most prevailing monosaccharide among *d*FCHO in seawater, ranged between 0.6 and 51 $\mu g\,L^{-1}$ during the PS106 cruise in the bulk and the SML (Zeppenfeld et al., 2019a). Thus, *d*FCHO / CHO ratios, meaning the contribution of sugar monomers to all marine carbohydrates measured in this study, varied between 1 %–14 % with an average of 5 ± 3 %. Conversely, 86 %–99 % (mean: 95 ± 3) of carbohydrates in the bulk and SML of ocean seawater and melt ponds were incorporated into an oligo- or polysaccharidic structure. CCHO can be hydrolyzed to *d*FCHO either in an acidic environment or enzymatically by heterotrophic bacteria (Arnosti, 2000; Panagiotopoulos and Sempéré, 2005). Seawater from the Arctic Ocean is slightly alkaline with reported pH values between 7.98 and 8.49 (Rérolle et al., 2016; Tynan et al., 2016), while the pH of melt pond water has been observed to be more variable from mildly acidic (6.1) to more alkaline (10.8) (Bates et al., 2014). In agreement with previous findings, the oceanic surface seawater (pH: 7.98–8.66), including the samples from the MIZ, ice-free ocean and open leads and polynyas, and the melt pond samples (pH: 7.26–8.62) were slightly alkaline in this study. Consequently, it is more plausible that the depolymerization of CCHO in seawater can be ascribed to bacterial activities rather than acid hydrolysis. Since *d*FCHO is readily resorbed by heterotrophic bacteria with high turnover rates (Ittekkot et al., 1981; Kirchman et al., 2001), concentrations of these monosaccharides are rather low in seawater.

In contrast, in aerosol particles, higher *d*FCHO / CHO ratios up to 35 % occurred in some selected samples, which is much higher than in seawater, suggesting that CCHO might be depolymerized in the atmosphere. SSA particles are known to significantly acidify within minutes after their release due to the uptake of acidic gases, atmospheric aging reactions with sulfuric dioxide and water loss (Angle et al., 2021). In this context, the surface-to-volume ratio determines the efficiency of the acidification effect, which means that it is most pronounced for submicron SSA particles with reported pH values of 1.5–2.6 within a few minutes in a tank study (Angle et al., 2021) and less pronounced for supermicron SSA particles or cloud droplets (Angle et al., 2022). Consequently, it is conceivable that an acid hydrolysis of $CCHO_{aer}$ to monomeric $dFCHO_{aer}$ occurs at the surface or within the bulk of SSA particles leading to quick atmospheric aging. However, due to analytical constraints, such as the limits of detections (LODs) of the methodology, the *d*FCHO in size-resolved aerosol particles could not be detected in all samples, and the data availability is not strong enough to draw more conclusions for aerosol particles.

In fog, where LODs did not represent an issue due to the high concentrations, *d*FCHO / CHO ratios exceeding those in seawater were also observed, ranging from 1 %–60 % (mean: 27 ± 16 %). The monosaccharide composition of $dFCHO_{fog}$ was primarily made up of glucose, arabinose, fructose and xylose, with minor contributions from glucosamine, galactose, mannose, rhamnose and fucose. While $dFCHO_{fog}$ and $CCHO_{fog}$ shared similar dominant monosaccharides, fructose was only present in $dFCHO_{fog}$. This absence in $CCHO_{fog}$ is attributed to fructose's low stability during the analytical preparation for CCHO analysis (Panagiotopoulos and Sempéré, 2005). As a result, fructose will not be further discussed. In this study, pH values of fog water ranged between 5.7 and 6.8, which is 1–2 magnitudes more acidic than in seawater. Polysaccharides are known to depolymerize due to acid hydrolysis, especially at elevated temperatures. The pH stability can be largely variable among the different polysaccharides; however, we are not aware of studies that have shown such fast depolymerizations, in the sense of timescales relevant for atmospheric lifetime of aerosol particles, at such mildly acidic conditions and low temperatures as those of the Arctic atmosphere. Furthermore, there was no significant correlation between the pH and the *d*FCHO / CHO of these cloud samples. Consequently, there are no indications that the majority of CCHO was hydrolyzed inside the cloud droplets. However, it might be conceivable that hydrolysis had readily occurred within the non-activated SSA particle where pH values were much lower.

Besides an acid hydrolysis induced by quick atmospheric acidification of SSA particles, atmospheric radicals, such as OH (Trueblood et al., 2019), or photolytic cleavages of glycosidic bonds (Kubota et al., 1976) could have contributed to the degradation of atmospheric CCHO to monomeric *d*FCHO in SSA and marine fog. For these processes, however, still hardly any systematic lab studies have been conducted for the plurality of marine polysaccharides, which makes a classification of the meaning of these processes difficult. A preferred sea–air transfer of *d*FCHO over CCHO to explain this observation seems unlikely based on the missing enrichment of neutral *d*FCHO in contrast to the high EF_{aer} of CCHO shown in tank studies (Hasenecz et al., 2019, 2020). Finally, a microbial depolymerization of CCHO by extracellular enzymes in fog cannot be entirely ruled out considering that the activity of some polysaccharide-degrading enzymes, such as α- and β-glucosidase, has been found to accelerate in seawater with increasing acidity (Piontek et al., 2010). However, this finding was conducted for a pH range only 0.3 pH units lower than the typical pH of seawater, and it is not clear whether this finding can be transferred to the more acidic conditions in aerosol particles and fog water.

Several aging processes in the atmosphere. We observed significant changes between the chemical composition of marine carbohydrates in the surface seawater, including the bulk and SML, and atmospheric carbohydrates, including aerosol particles and fog. Based on the changing monosaccharide composition pattern of CCHO with selective degradation and formation of specific monosaccharides within CCHO, we conclude that there are microbial or enzymatic activities within the aerosol particles of fog droplets. Furthermore, the increasing contribution of *d*FCHO to the total carbohydrate pool in fog and aerosol particles might be

attributed to a hydrolytic cleavage of the glycosidic linkages between monosaccharide units within the oligo- and polysaccharides after a quick atmospheric acidification of SSA particles. Consequently, atmospheric carbohydrates experience quick atmospheric aging, potentially due to both biological and abiotic processes, after their release from the ocean. Possibly, this could affect the CCN and INP properties of marine carbohydrates and hence the formation and properties of clouds.

3.6 Perspective assessment of CCHO via bio-optical parameters

The absorption of phytoplankton (a_{ph}) and CDOM (a_{CDOM}) are bio-optical parameters providing additional information about the chemical and microbiological history of the water masses within the particulate and dissolved phase, respectively. They can be measured on discrete water samples and can also be assessed as products from satellites (Lefering et al., 2017; Matsuoka et al., 2012, 2013; Röttgers et al., 2016). Here we tested whether a_{ph} or CDOM parameters correlate with CCHO in seawater to potentially enable the remote-sensing approximation of marine CCHO in seawater and potentially in the atmosphere.

Good assessment of CCHO in seawater via $a_{ph}440$. $a_{ph}440$ derived from the phytoplankton absorption spectrum is directly related to the biomarker TChl *a* indicating phytoplankton biomass (Bricaud et al., 2004; Phongphattarawat, 2016). The advantage of using $a_{ph}440$ over pigment data, including TChl *a* from full high-performance liquid chromatography (HPLC) analysis (e.g., Barlow et al., 1997; Taylor et al., 2011), is the lower need of sample volume for the analysis. This allows the determination of values in the SML samples as well (Zäncker et al., 2017), which are laborious to collect and therefore limited in availability. In this study, $a_{ph}440$ strongly correlated with *p*CCHO ($R = 0.90$, $p < 0.001$) in bulk and SML samples (Fig. 9a) showing a direct link with fresh phytoplankton biomass production. A similar link has been described before for TChl *a* and *p*CCHO in the photic layer of the Ross Sea (Fabiano et al., 1993), in the ocean west of the Antarctic Peninsula (Zeppenfeld et al., 2021a), and between TChl *a* and the particulate form of laminarin, an algal polysaccharide, in Arctic and Atlantic water samples (Becker et al., 2020). *d*CCHO showed a good but weaker correlation with $a_{ph}440$ ($R = 0.66$, $p < 0.001$) than *p*CCHO. This finding supports the assumption that *p*CCHO is rather freshly produced by local autotrophs, while the link between *d*CCHO with their primary production was already obscured by subsequent transformation processes resulting in a more recalcitrant, long-lived mix of macromolecules (Goldberg et al., 2011; Hansell, 2013; Keene et al., 2017). Nevertheless, CCHO, the sum from *d*CCHO and *p*CCHO, showed a high correlation with $a_{ph}440$ ($R = 0.84$, $p < 0.001$, Fig. 9b), leading to the conclusion that this bio-optical parameter derived from the $a_{ph}(\lambda)$ spectrum is suitable to assess the total amount of CCHO in the surface seawater of the different sea-ice-related sea surface compartments of the Arctic.

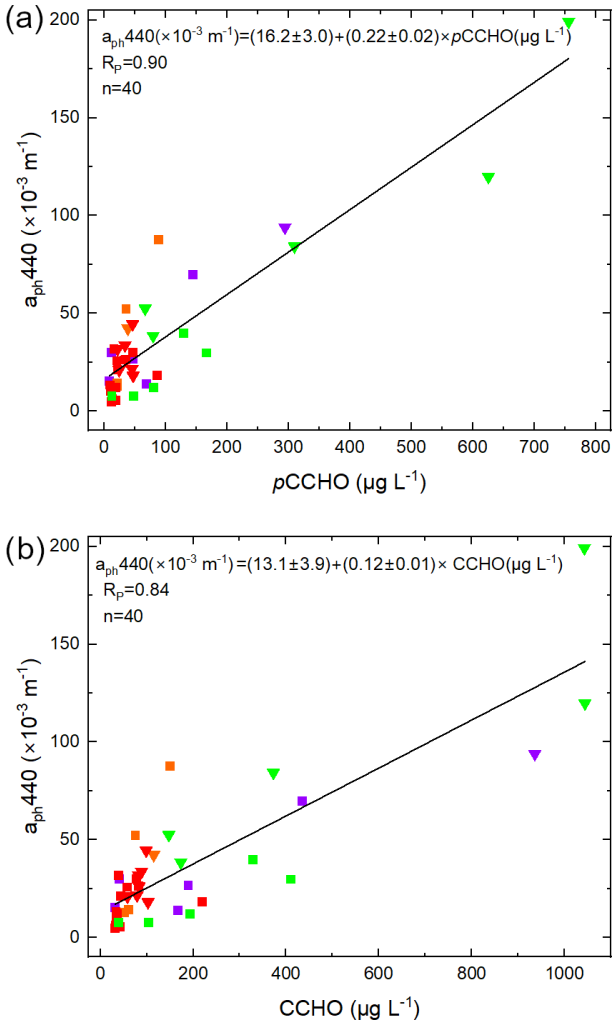

Figure 9. Correlation plots of $a_{ph}440$ derived from PAB spectra against **(a)** *p*CCHO and **(b)** CCHO. Triangles: SML, squares: bulk. Green: marginal ice zone (MIZ), purple: melt ponds, orange: ice-free ocean, red: open leads and polynyas in the pack ice.

Good assessment of CCHO in seawater via $a_{CDOM}350$. In this study, high correlations were observed between *d*CCHO and $a_{CDOM}350$ ($R = 0.66$, $p < 0.001$, Fig. 10a) and weaker correlations between *d*CCHO and $a_{CDOM}443$ ($R = 0.53$, $p < 0.001$, Fig. 10b). The better correlation at $\lambda = 350$ nm compared to 443 nm can be explained by the fact that a_{CDOM} exponentially decreases with wavelength. While absorption by CDOM is higher at $\lambda = 350$ nm, it is much closer to the method detection limit at $\lambda = 443$ nm and is therefore more error-prone. However, with current satellite products only a_{CDOM} at 440 nm can be retrieved.

Previous studies reported strong correlations between $a_{CDOM}350$ and dissolved organic carbon (DOC) in Arc-

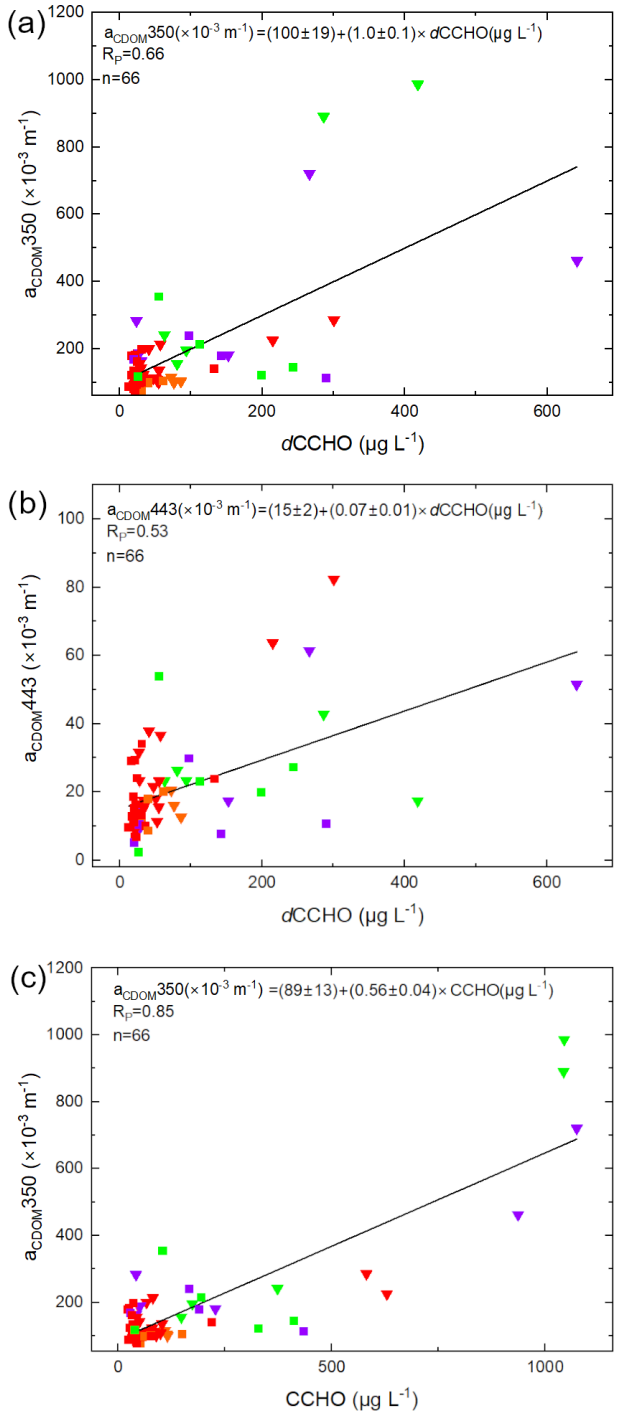

Figure 10. Correlation plots of **(a)** $a_{CDOM}350$ against dCCHO, **(b)** $a_{CDOM}443$ against dCCHO and **(c)** $a_{CDOM}350$ against CCHO. Triangles: SML, squares: bulk. Green: marginal ice zone (MIZ), purple: melt ponds, orange: ice-free ocean, red: open leads and polynyas in the pack ice.

tic seawater (Gonçalves-Araujo et al., 2015; Spencer et al., 2009; Stedmon et al., 2011; Walker et al., 2013). Consequently, it is conceivable that dCCHO, an important constituent of DOC, shows good correlations as well. Surprisingly, the correlation between CCHO (sum of dCCHO and pCCHO) and $a_{CDOM}350$ was strongest ($R = 0.85$, $p < 0.001$, Fig. 10c), indicating that CDOM retrieval from high-resolution satellite data could allow a good approximation of CCHO in Arctic seawater.

4 Summary and atmospheric implications

We studied the sea–air transfer of marine carbohydrates from field samples collected in the Arctic during the PS106 campaign from May to July 2017. Large differences of absolute CCHO concentrations and SML enrichments were observed among the different sea-ice-related sea surface compartments (leads and polynyas within the pack ice, ice-free ocean, MIZ, melt ponds). $CCHO_{aer}$ was detected in the sub- and supermicron aerosol particles with indications for primary emissions from the sea through bubble bursting, though the correlations with the SSA tracer Na^+ and wind speed were possibly reduced due to the presence of sea ice influencing the wind-induced SSA emission mechanisms. Atmospheric CCHO and Na^+ concentrations in fog strongly exceeded those of the aerosol particles likely due to a physical phenomenon. Large enrichments of CCHO in aerosol and fog compared to bulk seawater were observed. The extent of these enrichments varied based on the type of sea-ice-related sea surface compartment assumed as the oceanic source for atmospheric CCHO. We observed a subsequent atmospheric aging of CCHO in the atmosphere, both in aerosol particles and fog, noticed by the selective loss and formation of certain monosaccharide units within CCHO suggesting selective enzymatic/microbial activities, and a depolymerization of CCHO to dFCHO, most measurable in fog water and likely due to abiotic degradation, e.g., acid hydrolysis. CCHO correlated well with bio-optical parameters, such as $a_{ph}440$ from phytoplankton absorption and $a_{CDOM}350$. These parameters can be measured via remote sensing and may allow the retrieval of CCHO from satellite data, which potentially will enable an accurate modeling of atmospheric CCHO concentrations as soon as all emission and atmospheric aging processes are sufficiently understood. This study shows that the Arctic is a complex environment, where the diversity of sea-ice-related sea surface compartments needs to be considered as primary sources of marine CCHO or other organic compounds, and where these molecules can be transformed after their primary sea–air transfer by biological and abiotic processes in the atmosphere.

Marine carbohydrates are assumed to impact cloud properties by acting as CCN and INP (Alpert et al. 2022; Leck et al., 2013; Orellana et al., 2011; van Pinxteren et al., 2022). Studying the chemical identity of those atmospheric nucleation particles, their emission mechanisms and their transformation due to atmospheric aging can strongly improve the understanding of the cloud formation in the Arc-

tic, cloud microphysical properties, the radiation budget, cryosphere–ocean–atmosphere interactions and eventually feedback mechanisms in the frame of Arctic amplification. It can be assumed that within the warming Arctic, where sea ice extent is continuously shrinking, the MIZ area will expand (Strong and Rigor, 2013) and the number of biologically active melt ponds will increase during the summer season in the next years. These new MIZ regions and melt ponds could potentially produce more marine carbohydrates than the ice-free ocean or open leads within the pack ice, leading to enhanced CCN and INP populations in the Arctic atmosphere serving as a still not well-explored feedback mechanism within Arctic amplification.

Appendix A: List of abbreviations

a_{CDOM}	absorption coefficient by colored dissolved organic carbon
aer	aerosol particles
a_{NAP}	absorption coefficient by non-algal particles
ANOVA	analysis of variance
a_p	absorption coefficient by total particles
a_{ph}	absorption coefficient by phytoplankton
Ara	arabinose
atmos	atmospheric concentrations
C–CCHO	carbon contained within the combined carbohydrates
CCHO	combined carbohydrates
CCN	cloud condensation nuclei
CDOM	colored dissolved organic matter
CHO	carbohydrates
*d*CCHO	dissolved combined carbohydrates
*d*FCHO	dissolved free carbohydrates
EF	enrichment factor
EPS	exopolymeric substance
ERDDAP	Environmental Research Division's Data Access Program
FAA	free amino acid
Fru	fructose
Fuc	fucose
Gal	galactose
GalN	galactosamine
GalAc	galacturonic acid
Glc	glucose
GlcAc	glucuronic acid
GlcN	glucosamine
HPAEC-PAD	high-performance anion-exchange chromatography with pulsed amperometric detection
HPLC	high-performance liquid chromatography
INP	ice-nucleating particles
LWCC	liquid waveguide capillary cell
Man	mannose
MIZ	marginal ice zone
MurAc	muramic acid
Na^+	sodium ion
NOAA	National Oceanic and Atmospheric Administration
OC	organic carbon
OM	organic matter
PAB	particulate absorption
*p*CCHO	particulate combined carbohydrates
PM	particulate matter
Rha	rhamnose
SML	sea surface microlayer
SSA	sea spray aerosol
sub	submicron
super	supermicron
TChl *a*	total chlorophyll *a*
TEP	transparent exopolymer particles
QFT-ICAM	quantitative filtration technique with an integrative cavity absorption meter setup
Xyl	xylose

Data availability. All data are available on the public repository PANGAEA: https://doi.org/10.1594/PANGAEA.962208 (Zeppenfeld et al., 2023a) and https://doi.org/10.1594/PANGAEA.932573 (Zeppenfeld et al., 2021c) (for fog samples), https://doi.org/10.1594/PANGAEA.962210 (Zeppenfeld et al., 2023b) and https://doi.org/10.1594/PANGAEA.932569 (Zeppenfeld et al., 2021d) (for aerosol particles), and https://doi.org/10.1594/PANGAEA.961004 (Zeppenfeld et al., 2023c) (for seawater samples).

Video supplement. Daily sea ice maps for PS106 showing sea ice concentrations (SIC) and 120 h back trajectories on an hourly basis at three arrival heights (50, 250 and 1000 m) are available online at https://doi.org/10.5446/62589 (Zeppenfeld, 2023).

Supplement. The supplement related to this article is available online at: https://doi.org/10.5194/acp-23-15561-2023-supplement.

Author contributions. SZ wrote the manuscript with contributions from MvP, MH, MZ, AB and HaH. SZ, MvP and MH collected the field samples during the PS106 campaign. SZ performed the laboratory carbohydrate analysis and statistical evaluation. MZ and AB assessed the bio-optical parameters. All co-authors proofread and commented on the manuscript.

Competing interests. The contact author has declared that none of the authors has any competing interests.

Disclaimer. Publisher's note: Copernicus Publications remains neutral with regard to jurisdictional claims made in the text, published maps, institutional affiliations, or any other geographical representation in this paper. While Copernicus Publications makes every effort to include appropriate place names, the final responsibility lies with the authors.

Acknowledgements. We gratefully acknowledge the funding by the Deutsche Forschungsgemeinschaft (DFG, German Research Foundation, project no. 268020496−TRR 172) within the Transregional Collaborative Research Center "ArctiC Amplification: Climate Relevant Atmospheric and SurfaCe Processes, and Feedback Mechanisms $(AC)^3$" in subprojects B04 and C03. This research has been supported by the DFG SPP 1158 (grant no. 424326801) by enabling the access to melt pond data. We thank Andreas Macke and Hauke Flores, chief scientists for the RV *Polarstern* cruises PS106.1 and PS106.2 (expedition grant no. AWI_PS106_00), and the captain and the crew of RV *Polarstern* for their support during the expedition from May to July 2017. We thank Andrea Haudek and Hartmut Haudek for the development and construction of the conditioning tube and the wind control system connected to the Berner impactor. We thank Anett Dietze, Susanne Fuchs and Anke Rödger for the mass, inorganic ion and OC / EC measurements. We acknowledge René Rabe and Sonja Wiegmann for supporting the prepara-

tion of PS106 chemical equipment and optical instrumentation, respectively, and Yangyang Liu for introducing the optical measurement procedure before PS106.

Financial support. This research has been supported by the Deutsche Forschungsgemeinschaft (DFG, German Research Foundation, project no. 268020496-TRR 172) within the Transregional Collaborative Research Center "ArctiC Amplification: Climate Relevant Atmospheric and SurfaCe Processes, and Feedback Mechanisms $(AC)^3$" in subprojects B04 and C03.

Review statement. This paper was edited by Alex Huffman and reviewed by two anonymous referees.

References

Alderkamp, A.-C., Buma, A. G. J., and van Rijssel, M.: The carbohydrates of Phaeocystis and their degradation in the microbial food web, Biogeochemistry, 83, 99–118, https://doi.org/10.1007/s10533-007-9078-2, 2007.

Aller, J. Y., Kuznetsova, M. R., Jahns, C. J., and Kemp, P. F.: The sea surface microlayer as a source of viral and bacterial enrichment in marine aerosols, J. Aerosol Sci., 36, 801–812, https://doi.org/10.1016/j.jaerosci.2004.10.012, 2005.

Aller, J. Y., Radway, J. C., Kilthau, W. P., Bothe, D. W., Wilson, T. W., Vaillancourt, R. D., Quinn, P. K., Coffman, D. J., Murray, B. J., and Knopf, D. A.: Size-resolved characterization of the polysaccharidic and proteinaceous components of sea spray aerosol, Atmos. Environ., 154, 331–347, https://doi.org/10.1016/j.atmosenv.2017.01.053, 2017.

Alpert, P. A., Kilthau, W. P., O'Brien, R. E., Moffet, R. C., Gilles, M. K., Wang, B., Laskin, A., Aller, J. Y., and Knopf, D. A.: Ice-nucleating agents in sea spray aerosol identified and quantified with a holistic multimodal freezing model, Science Advances, 8, eabq6842, https://doi.org/10.1126/sciadv.abq6842, 2022.

Álvarez, E., Losa, S. N., Bracher, A., Thoms, S., and Völker, C.: Phytoplankton Light Absorption Impacted by Photoprotective Carotenoids in a Global Ocean Spectrally-Resolved Biogeochemistry Model, J. Adv. Model. Earth Sy., 14, e2022MS003126, https://doi.org/10.1029/2022MS003126, 2022.

Amon, R. M. W., Fitznar, H.-P., and Benner, R.: Linkages among the bioreactivity, chemical composition, and diagenetic state of marine dissolved organic matter, Limnol. Oceanogr., 46, 287–297, 2001.

Angle, K., Grassian, V. H., and Ault, A. P.: The rapid acidification of sea spray aerosols, Phys. Today, 75, 58–59, https://doi.org/10.1063/PT.3.4926, 2022.

Angle, K. J., Crocker, D. R., Simpson, R. M. C., Mayer, K. J., Garofalo, L. A., Moore, A. N., Garcia, S. L. M., Or, V. W., Srinivasan, S., Farhan, M., Sauer, J. S., Lee, C., Pothier, M. A., Farmer, D. K., Martz, T. R., Bertram, T. H., Cappa, C. D., Prather, K. A., and Grassian, V. H.: Acidity across the interface from the ocean surface to sea spray aerosol, P. Natl. Acad. Sci. USA, 118, e2018397118, https://doi.org/10.1073/pnas.2018397118, 2021.

Arnosti, C.: Substrate specificity in polysaccharide hydrolysis: Contrasts between bottom water and sediments, Limnol. Oceanogr., 45, 1112–1119, https://doi.org/10.4319/lo.2000.45.5.1112, 2000.

Aslam, S. N., Michel, C., Niemi, A., and Underwood, G. J. C.: Patterns and drivers of carbohydrate budgets in ice algal assemblages from first year Arctic sea ice, Limnol. Oceanogr., 61, 919–937, https://doi.org/10.1002/lno.10260, 2016.

Azetsu-Scott, K. and Passow, U.: Ascending marine particles: Significance of transparent exopolymer particles (TEP) in the upper ocean, Limnol. Oceanogr., 49, 741–748, https://doi.org/10.4319/lo.2004.49.3.0741, 2004.

Barlow, R., Cummings, D., and Gibb, S.: Improved resolution of mono- and divinyl chlorophylls a and b and zeaxanthin and lutein in phytoplankton extracts using reverse phase C-8 HPLC, Mar. Ecol. Prog. Ser., 161, 303–307, https://doi.org/10.3354/meps161303, 1997.

Barthel, S., Tegen, I., and Wolke, R.: Do new sea spray aerosol source functions improve the results of a regional aerosol model?, Atmos. Environ., 198, 265–278, https://doi.org/10.1016/j.atmosenv.2018.10.016, 2019.

Bates, N. R., Garley, R., Frey, K. E., Shake, K. L., and Mathis, J. T.: Sea-ice melt CO_2–carbonate chemistry in the western Arctic Ocean: meltwater contributions to air–sea CO_2 gas exchange, mixed-layer properties and rates of net community production under sea ice, Biogeosciences, 11, 6769–6789, https://doi.org/10.5194/bg-11-6769-2014, 2014.

Becker, S., Tebben, J., Coffinet, S., Wiltshire, K., Iversen, M. H., Harder, T., Hinrichs, K.-U., and Hehemann, J.-H.: Laminarin is a major molecule in the marine carbon cycle, P. Natl. Acad. Sci. USA, 117, 6599–6607, https://doi.org/10.1073/pnas.1917001117, 2020.

Benner, R. and Kaiser, K.: Abundance of amino sugars and peptidoglycan in marine particulate and dissolved organic matter, Limnol. Oceanogr., 48, 118–128, https://doi.org/10.4319/lo.2003.48.1.0118, 2003.

Bigg, E. K. and Leck, C.: The composition of fragments of bubbles bursting at the ocean surface, J. Geophys. Res.-Atmos., 113, D11209, https://doi.org/10.1029/2007JD009078, 2008.

Bikerman, J. J.: Foams, Springer Science & Business Media, 344 pp., https://doi.org/10.1007/978-3-642-86734-7, 2013.

Bozem, H., Hoor, P., Kunkel, D., Köllner, F., Schneider, J., Herber, A., Schulz, H., Leaitch, W. R., Aliabadi, A. A., Willis, M. D., Burkart, J., and Abbatt, J. P. D.: Characterization of transport regimes and the polar dome during Arctic spring and summer using in situ aircraft measurements, Atmos. Chem. Phys., 19, 15049–15071, https://doi.org/10.5194/acp-19-15049-2019, 2019.

Bricaud, A., Claustre, H., Ras, J., and Oubelkheir, K.: Natural variability of phytoplanktonic absorption in oceanic waters: Influence of the size structure of algal populations, J. Geophys. Res.-Oceans, 109, C11010. https://doi.org/10.1029/2004JC002419, 2004.

Burrows, S. M., Ogunro, O., Frossard, A. A., Russell, L. M., Rasch, P. J., and Elliott, S. M.: A physically based framework for modeling the organic fractionation of sea spray aerosol from bubble film Langmuir equilibria, Atmos. Chem. Phys., 14, 13601–13629, https://doi.org/10.5194/acp-14-13601-2014, 2014.

Burrows, S. M., Gobrogge, E., Fu, L., Link, K., Elliott, S. M., Wang, H., and Walker, R.: OCEANFILMS-2: Representing coadsorption of saccharides in marine films and potential impacts on modeled marine aerosol chemistry, Geophys. Res. Lett., 43, 8306–8313, https://doi.org/10.1002/2016GL069070, 2016.

Callaghan, A. H., Deane, G. B., Stokes, M. D., and Ward, B.: Observed variation in the decay time of oceanic whitecap foam, J. Geophys. Res.-Oceans, 117, C09015, https://doi.org/10.1029/2012JC008147, 2012.

Casillo, A., Lanzetta, R., Parrilli, M., and Corsaro, M. M.: Exopolysaccharides from Marine and Marine Extremophilic Bacteria: Structures, Properties, Ecological Roles and Applications, Mar. Drugs, 16, 69, https://doi.org/10.3390/md16020069, 2018.

Chen, Q., Mirrielees, J. A., Thanekar, S., Loeb, N. A., Kirpes, R. M., Upchurch, L. M., Barget, A. J., Lata, N. N., Raso, A. R. W., McNamara, S. M., China, S., Quinn, P. K., Ault, A. P., Kennedy, A., Shepson, P. B., Fuentes, J. D., and Pratt, K. A.: Atmospheric particle abundance and sea salt aerosol observations in the springtime Arctic: a focus on blowing snow and leads, Atmos. Chem. Phys., 22, 15263–15285, https://doi.org/10.5194/acp-22-15263-2022, 2022.

Chi, J. W., Li, W. J., Zhang, D. Z., Zhang, J. C., Lin, Y. T., Shen, X. J., Sun, J. Y., Chen, J. M., Zhang, X. Y., Zhang, Y. M., and Wang, W. X.: Sea salt aerosols as a reactive surface for inorganic and organic acidic gases in the Arctic troposphere, Atmos. Chem. Phys., 15, 11341–11353, https://doi.org/10.5194/acp-15-11341-2015, 2015.

Creamean, J. M., Barry, K., Hill, T. C. J., Hume, C., DeMott, P. J., Shupe, M. D., Dahlke, S., Willmes, S., Schmale, J., Beck, I., Hoppe, C. J. M., Fong, A., Chamberlain, E., Bowman, J., Scharien, R., and Persson, O.: Annual cycle observations of aerosols capable of ice formation in central Arctic clouds, Nat. Commun., 13, 3537, https://doi.org/10.1038/s41467-022-31182-x, 2022.

Cunliffe, M. and Wurl, O.: Guide to best practices to study the ocean's surface., Marine Biological Association of the United Kingdom for SCOR, https://repository.oceanbestpractices.org/bitstream/handle/11329/261/SCOR_GuideSeaSurface_2014.pdf?sequence=1&isAllowed=y (last access: 3 February 2022), 2014.

Cunliffe, M., Engel, A., Frka, S., Gašparović, B., Guitart, C., Murrell, J. C., Salter, M., Stolle, C., Upstill-Goddard, R., and Wurl, O.: Sea surface microlayers: A unified physicochemical and biological perspective of the air–ocean interface, Prog. Oceanogr., 109, 104–116, https://doi.org/10.1016/j.pocean.2012.08.004, 2013.

Delort, A.-M., Vaïtilingom, M., Amato, P., Sancelme, M., Parazols, M., Mailhot, G., Laj, P., and Deguillaume, L.: A short overview of the microbial population in clouds: Potential roles in atmospheric chemistry and nucleation processes, Atmos. Res., 98, 249–260, https://doi.org/10.1016/j.atmosres.2010.07.004, 2010.

DeMott, P. J., Hill, T. C. J., McCluskey, C. S., Prather, K. A., Collins, D. B., Sullivan, R. C., Ruppel, M. J., Mason, R. H., Irish, V. E., Lee, T., Hwang, C. Y., Rhee, T. S., Snider, J. R., McMeeking, G. R., Dhaniyala, S., Lewis, E. R., Wentzell, J. J. B., Abbatt, J., Lee, C., Sultana, C. M., Ault, A. P., Axson, J. L., Martinez, M. D., Venero, I., Santos-Figueroa, G., Stokes, M. D., Deane, G. B., Mayol-Bracero, O. L., Grassian, V. H., Bertram, T. H., Bertram, A. K., Moffett, B. F., and Franc, G. D.: Sea spray aerosol as a unique source of ice nucleating particles, P. Natl. Acad. Sci. USA, 113, 5797–5803, https://doi.org/10.1073/pnas.1514034112, 2016.

Demoz, B. B., Collett, J. L., and Daube, B. C.: On the Caltech Active Strand Cloudwater Collectors, Atmos. Res., 41, 47–62, https://doi.org/10.1016/0169-8095(95)00044-5, 1996.

Dominutti, P. A., Renard, P., Vaïtilingom, M., Bianco, A., Baray, J.-L., Borbon, A., Bourianne, T., Burnet, F., Colomb, A., Delort, A.-M., Duflot, V., Houdier, S., Jaffrezo, J.-L., Joly, M., Leremboure, M., Metzger, J.-M., Pichon, J.-M., Ribeiro, M., Rocco, M., Tulet, P., Vella, A., Leriche, M., and Deguillaume, L.: Insights into tropical cloud chemistry in Réunion (Indian Ocean): results from the BIO-MAÏDO campaign, Atmospheric Chemistry and Physics, 22, 505–533, https://doi.org/10.5194/acp-22-505-2022, 2022.

Engbrodt, R.: Biogeochemistry of dissolved carbohydrates in the Arctic, Berichte zur Polar-und Meeresforschung (Reports on Polar and Marine Research), 396, 106 pp., https://epic.awi.de/id/eprint/26575/1/BerPolarforsch2001396.pdf (last access: 13 January 2021), 2001.

Engel, A. and Händel, N.: A novel protocol for determining the concentration and composition of sugars in particulate and in high molecular weight dissolved organic matter (HMW-DOM) in seawater, Mar. Chem., 127, 180–191, https://doi.org/10.1016/j.marchem.2011.09.004, 2011.

Engel, A., Bange, H. W., Cunliffe, M., Burrows, S. M., Friedrichs, G., Galgani, L., Herrmann, H., Hertkorn, N., Johnson, M., Liss, P. S., Quinn, P. K., Schartau, M., Soloviev, A., Stolle, C., Upstill-Goddard, R. C., van Pinxteren, M., and Zäncker, B.: The Ocean's Vital Skin: Toward an Integrated Understanding of the Sea Surface Microlayer, Front. Mar. Sci., 4, 165, https://doi.org/10.3389/fmars.2017.00165, 2017.

Ervens, B. and Amato, P.: The global impact of bacterial processes on carbon mass, Atmos. Chem. Phys., 20, 1777–1794, https://doi.org/10.5194/acp-20-1777-2020, 2020.

Fabiano, M., Povero, P., and Danovaro, R.: Distribution and composition of particulate organic matter in the Ross Sea (Antarctica), Polar Biol., 13, 525–533, https://doi.org/10.1007/BF00236394, 1993.

Facchini, M. C., Rinaldi, M., Decesari, S., Carbone, C., Finessi, E., Mircea, M., Fuzzi, S., Ceburnis, D., Flanagan, R., Nilsson, E. D., de Leeuw, G., Martino, M., Woeltjen, J., and O'Dowd, C. D.: Primary submicron marine aerosol dominated by insoluble organic colloids and aggregates, Geophys. Res. Lett., 35, L17814, https://doi.org/10.1029/2008GL034210, 2008.

Galgani, L., Piontek, J., and Engel, A.: Biopolymers form a gelatinous microlayer at the air-sea interface when Arctic sea ice melts, Sci. Rep., 6, 29465, https://doi.org/10.1038/srep29465, 2016.

Gantt, B., Meskhidze, N., Facchini, M. C., Rinaldi, M., Ceburnis, D., and O'Dowd, C. D.: Wind speed dependent size-resolved parameterization for the organic mass fraction of sea spray aerosol, Atmos. Chem. Phys., 11, 8777–8790, https://doi.org/10.5194/acp-11-8777-2011, 2011.

Gao, Q., Leck, C., Rauschenberg, C., and Matrai, P. A.: On the chemical dynamics of extracellular polysaccharides in the high Arctic surface microlayer, Ocean Sci., 8, 401–418, https://doi.org/10.5194/os-8-401-2012, 2012.

Gilardoni, S., Massoli, P., Giulianelli, L., Rinaldi, M., Paglione, M., Pollini, F., Lanconelli, C., Poluzzi, V., Carbone, S., Hillamo,

R., Russell, L. M., Facchini, M. C., and Fuzzi, S.: Fog scavenging of organic and inorganic aerosol in the Po Valley, Atmos. Chem. Phys., 14, 6967–6981, https://doi.org/10.5194/acp-14-6967-2014, 2014.

Goldberg, S. J., Carlson, C. A., Brzezinski, M., Nelson, N. B., and Siegel, D. A.: Systematic removal of neutral sugars within dissolved organic matter across ocean basins, Geophys. Res. Lett., 38, L17606, https://doi.org/10.1029/2011GL048620, 2011.

Gonçalves-Araujo, R., Stedmon, C. A., Heim, B., Dubinenkov, I., Kraberg, A., Moiseev, D., and Bracher, A.: From Fresh to Marine Waters: Characterization and Fate of Dissolved Organic Matter in the Lena River Delta Region, Siberia, Frontiers in Marine Science, 2, 108, https://doi.org/10.3389/fmars.2015.00108, 2015.

Gong, X., Zhang, J., Croft, B., Yang, X., Frey, M. M., Bergner, N., Chang, R. Y.-W., Creamean, J. M., Kuang, C., Martin, R. V., Ranjithkumar, A., Sedlacek, A. J., Uin, J., Willmes, S., Zawadowicz, M. A., Pierce, J. R., Shupe, M. D., Schmale, J., and Wang, J.: Arctic warming by abundant fine sea salt aerosols from blowing snow, Nat. Geosci., 16, 768–774, https://doi.org/10.1038/s41561-023-01254-8, 2023.

Grythe, H., Ström, J., Krejci, R., Quinn, P., and Stohl, A.: A review of sea-spray aerosol source functions using a large global set of sea salt aerosol concentration measurements, Atmos. Chem. Phys., 14, 1277–1297, https://doi.org/10.5194/acp-14-1277-2014, 2014.

Haddrell, A. E. and Thomas, R. J.: Aerobiology: Experimental Considerations, Observations, and Future Tools, Appl. Environ. Microb., 83, e00809-17, https://doi.org/10.1128/AEM.00809-17, 2017.

Hansell, D. A.: Recalcitrant Dissolved Organic Carbon Fractions, Annu. Rev. Mar. Sci., 5, 421–445, https://doi.org/10.1146/annurev-marine-120710-100757, 2013.

Hara, K., Yamagata, S., Yamanouchi, T., Sato, K., Herber, A., Iwasaka, Y., Nagatani, M., and Nakata, H.: Mixing states of individual aerosol particles in spring Arctic troposphere during ASTAR 2000 campaign, J. Geophys. Res.-Atmos., 108, 4209, https://doi.org/10.1029/2002JD002513, 2003.

Hartmann, M., Gong, X., Kecorius, S., van Pinxteren, M., Vogl, T., Welti, A., Wex, H., Zeppenfeld, S., Herrmann, H., Wiedensohler, A., and Stratmann, F.: Terrestrial or marine – indications towards the origin of ice-nucleating particles during melt season in the European Arctic up to 83.7° N, Atmos. Chem. Phys., 21, 11613–11636, https://doi.org/10.5194/acp-21-11613-2021, 2021.

Hasenecz, E., Jayarathne, T., Pendergraft, M. A., Santander, M. V., Mayer, K. J., Sauer, J., Lee, C., Gibson, W. S., Kruse, S. M., Malfatti, F., Prather, K. A., and Stone, E. A.: Marine bacteria affect saccharide enrichment in sea spray aerosol during a phytoplankton bloom, ACS Earth Space Chem., 4, 1638–1649, https://doi.org/10.1021/acsearthspacechem.0c00167, 2020.

Hasenecz, E. S., Kaluarachchi, C. P., Lee, H. D., Tivanski, A. V., and Stone, E. A.: Saccharide Transfer to Sea Spray Aerosol Enhanced by Surface Activity, Calcium, and Protein Interactions, ACS Earth Space Chem., 3, 2539–2548, https://doi.org/10.1021/acsearthspacechem.9b00197, 2019.

Held, A., Brooks, I. M., Leck, C., and Tjernström, M.: On the potential contribution of open lead particle emissions to the central Arctic aerosol concentration, Atmos. Chem. Phys., 11, 3093–3105, https://doi.org/10.5194/acp-11-3093-2011, 2011.

Herrmann, H., Schaefer, T., Tilgner, A., Styler, S. A., Weller, C., Teich, M., and Otto, T.: Tropospheric Aqueous-Phase Chemistry: Kinetics, Mechanisms, and Its Coupling to a Changing Gas Phase, Chem. Rev., 115, 4259–4334, https://doi.org/10.1021/cr500447k, 2015.

Hoffman, E. J. and Duce, R. A.: Factors influencing the organic carbon content of marine aerosols: A laboratory study, J. Geophys. Res., 81, 3667–3670, https://doi.org/10.1029/JC081i021p03667, 1976.

Huang, J. and Jaeglé, L.: Wintertime enhancements of sea salt aerosol in polar regions consistent with a sea ice source from blowing snow, Atmos. Chem. Phys., 17, 3699–3712, https://doi.org/10.5194/acp-17-3699-2017, 2017.

Istomina, L., Marks, H., Niehaus, H., Huntemann, M., Heygster, G., and Spreen, G.: Retrieval of sea ice surface melt using OLCI data onboard Sentinel-3, AGU Fall Meeting, https://ui.adsabs.harvard.edu/abs/2020AGUFMC017...07I/abstract (last access: 20 April 2023), 2020.

Ittekkot, V., Brockmann, U., Michaelis, W., and Degens, E. T.: Dissolved free and combined carbohydrates during a phytoplankton bloom in the northern North Sea, Mar. Ecol. Prog. Ser., 4, 299–305, 1981.

Karl, M., Leck, C., Rad, F. M., Bäcklund, A., Lopez-Aparicio, S., and Heintzenberg, J.: New insights in sources of the sub-micrometre aerosol at Mt. Zeppelin observatory (Spitsbergen) in the year 2015, Tellus B, 71, 1613143, https://doi.org/10.1080/16000889.2019.1613143, 2019.

Kecorius, S., Vogl, T., Paasonen, P., Lampilahti, J., Rothenberg, D., Wex, H., Zeppenfeld, S., van Pinxteren, M., Hartmann, M., Henning, S., Gong, X., Welti, A., Kulmala, M., Stratmann, F., Herrmann, H., and Wiedensohler, A.: New particle formation and its effect on cloud condensation nuclei abundance in the summer Arctic: a case study in the Fram Strait and Barents Sea, Atmos. Chem. Phys., 19, 14339–14364, https://doi.org/10.5194/acp-19-14339-2019, 2019.

Keene, W. C., Long, M. S., Reid, J. S., Frossard, A. A., Kieber, D. J., Maben, J. R., Russell, L. M., Kinsey, J. D., Quinn, P. K., and Bates, T. S.: Factors That Modulate Properties of Primary Marine Aerosol Generated From Ambient Seawater on Ships at Sea, J. Geophys. Res.-Atmos., 122, 11961–11990, https://doi.org/10.1002/2017JD026872, 2017.

Kirchman, D. L., Meon, B., Ducklow, H. W., Carlson, C. A., Hansell, D. A., and Steward, G. F.: Glucose fluxes and concentrations of dissolved combined neutral sugars (polysaccharides) in the Ross Sea and Polar Front Zone, Antarctica, Deep-Sea Res. Pt. II, 48, 4179–4197, https://doi.org/10.1016/S0967-0645(01)00085-6, 2001.

Kirpes, R. M., Bondy, A. L., Bonanno, D., Moffet, R. C., Wang, B., Laskin, A., Ault, A. P., and Pratt, K. A.: Secondary sulfate is internally mixed with sea spray aerosol and organic aerosol in the winter Arctic, Atmos. Chem. Phys., 18, 3937–3949, https://doi.org/10.5194/acp-18-3937-2018, 2018.

Krembs, C. and Deming, J. W.: The role of exopolymers in microbial adaptation to sea ice, in: Psychrophiles: from biodiversity to biotechnology, Springer, 247–264, https://doi.org/10.1007/978-3-540-74335-4_15, 2008.

Krembs, C., Eicken, H., Junge, K., and Deming, J. W.: High concentrations of exopolymeric substances in Arctic winter sea ice: implications for the polar ocean carbon cycle and cry-

oprotection of diatoms, Deep-Sea Res. Pt. I, 49, 2163–2181, https://doi.org/10.1016/S0967-0637(02)00122-X, 2002.

Kubota, H., Ogiwara, Y., and Matsuzaki, K.: Photo-Induced Formation of Peroxide in Saccharides and Related Compounds, Polym. J., 8, 557–563, https://doi.org/10.1295/polymj.8.557, 1976.

Kumai, M.: Arctic Fog Droplet Size Distribution and Its Effect on Light Attenuation, J. Atmos. Sci., 30, 635–643, https://doi.org/10.1175/1520-0469(1973)030<0635:AFDSDA>2.0.CO;2, 1973.

Lawler, M. J., Saltzman, E. S., Karlsson, L., Zieger, P., Salter, M., Baccarini, A., Schmale, J., and Leck, C.: New Insights Into the Composition and Origins of Ultrafine Aerosol in the Summertime High Arctic, Geophys. Res. Lett., 48, e2021GL094395, https://doi.org/10.1029/2021GL094395, 2021.

Leck, C., Norman, M., Bigg, E. K., and Hillamo, R.: Chemical composition and sources of the high Arctic aerosol relevant for cloud formation, J. Geophys. Res., 107, 4135, https://doi.org/10.1029/2001JD001463, 2002.

Leck, C., Gao, Q., Mashayekhy Rad, F., and Nilsson, U.: Size-resolved atmospheric particulate polysaccharides in the high summer Arctic, Atmos. Chem. Phys., 13, 12573–12588, https://doi.org/10.5194/acp-13-12573-2013, 2013.

Lefering, I., Röttgers, R., Utschig, C., and McKee, D.: Uncertainty budgets for liquid waveguide CDOM absorption measurements, Appl. Opt., 56, 6357–6366, https://doi.org/10.1364/AO.56.006357, 2017.

Liu, Y., Röttgers, R., Ramírez-Pérez, M., Dinter, T., Steinmetz, F., Nöthig, E.-M., Hellmann, S., Wiegmann, S., and Bracher, A.: Underway spectrophotometry in the Fram Strait (European Arctic Ocean): a highly resolved chlorophyll *a* data source for complementing satellite ocean color, Opt. Express, 26, A678–A696, https://doi.org/10.1364/OE.26.00A678, 2018.

Macke, A. and Flores, H.: The Expeditions PS106/1 and 2 of the Research Vessel POLARSTERN to the Arctic Ocean in 2017, Bremerhaven, Germany, 171 pp., https://doi.org/10.2312/BzPM_0719_2018, 2018.

Malfatti, F., Lee, C., Tinta, T., Pendergraft, M. A., Celussi, M., Zhou, Y., Sultana, C. M., Rotter, A., Axson, J. L., Collins, D. B., Santander, M. V., Anides Morales, A. L., Aluwihare, L. I., Riemer, N., Grassian, V. H., Azam, F., and Prather, K. A.: Detection of Active Microbial Enzymes in Nascent Sea Spray Aerosol: Implications for Atmospheric Chemistry and Climate, Environ. Sci. Tech. Let., 6, 171–177, https://doi.org/10.1021/acs.estlett.8b00699, 2019.

Mari, X., Passow, U., Migon, C., Burd, A. B., and Legendre, L.: Transparent exopolymer particles: Effects on carbon cycling in the ocean, Prog. Oceanogr., 151, 13–37, https://doi.org/10.1016/j.pocean.2016.11.002, 2017.

Marks, R., Kruczalak, K., Jankowska, K., and Michalska, M.: Bacteria and fungi in air over the Gulf of Gdańsk and Baltic sea, J. Aerosol Sci., 32, 237–250, https://doi.org/10.1016/S0021-8502(00)00064-1, 2001.

Matsuoka, A., Bricaud, A., Benner, R., Para, J., Sempéré, R., Prieur, L., Bélanger, S., and Babin, M.: Tracing the transport of colored dissolved organic matter in water masses of the Southern Beaufort Sea: relationship with hydrographic characteristics, Biogeosciences, 9, 925–940, https://doi.org/10.5194/bg-9-925-2012, 2012.

Matsuoka, A., Hooker, S. B., Bricaud, A., Gentili, B., and Babin, M.: Estimating absorption coefficients of colored dissolved organic matter (CDOM) using a semi-analytical algorithm for southern Beaufort Sea waters: application to deriving concentrations of dissolved organic carbon from space, Biogeosciences, 10, 917–927, https://doi.org/10.5194/bg-10-917-2013, 2013.

Matulová, M., Husárová, S., Capek, P., Sancelme, M., and Delort, A.-M.: Biotransformation of Various Saccharides and Production of Exopolymeric Substances by Cloud-Borne *Bacillus* sp. 3B6, Environ. Sci. Technol., 48, 14238–14247, https://doi.org/10.1021/es501350s, 2014.

May, N. W., Quinn, P. K., McNamara, S. M., and Pratt, K. A.: Multiyear study of the dependence of sea salt aerosol on wind speed and sea ice conditions in the coastal Arctic: ARCTIC SEA SALT AEROSOL, J. Geophys. Res.-Atmos., 121, 9208–9219, https://doi.org/10.1002/2016JD025273, 2016.

Mayol, E., Arrieta, J. M., Jiménez, M. A., Martínez-Asensio, A., Garcias-Bonet, N., Dachs, J., González-Gaya, B., Royer, S.-J., Benítez-Barrios, V. M., Fraile-Nuez, E., and Duarte, C. M.: Long-range transport of airborne microbes over the global tropical and subtropical ocean, Nat. Commun., 8, 1–9, https://doi.org/10.1038/s41467-017-00110-9, 2017.

McCarthy, M., Hedges, J., and Benner, R.: Major biochemical composition of dissolved high molecular weight organic matter in seawater, Mar. Chem., 55, 281–297, https://doi.org/10.1016/S0304-4203(96)00041-2, 1996.

McCluskey, C. S., Hill, T. C. J., Humphries, R. S., Rauker, A. M., Moreau, S., Strutton, P. G., Chambers, S. D., Williams, A. G., McRobert, I., Ward, J., Keywood, M. D., Harnwell, J., Ponsonby, W., Loh, Z. M., Krummel, P. B., Protat, A., Kreidenweis, S. M., and DeMott, P. J.: Observations of Ice Nucleating Particles Over Southern Ocean Waters, Geophys. Res. Lett., 45, 11989–11997, https://doi.org/10.1029/2018GL079981, 2018.

Mimura, T. and Romano, J. C.: Muramic Acid measurements for bacterial investigations in marine environments by high-pressure liquid chromatography, Appl. Environ. Microb., 50, 229–237, https://doi.org/10.1128/AEM.50.2.229-237.1985, 1985.

Mühlenbruch, M., Grossart, H.-P., Eigemann, F., and Voss, M.: Mini-review: Phytoplankton-derived polysaccharides in the marine environment and their interactions with heterotrophic bacteria, Environ. Microbiol., 20, 2671–2685, https://doi.org/10.1111/1462-2920.14302, 2018.

Müller, K., Lehmann, S., van Pinxteren, D., Gnauk, T., Niedermeier, N., Wiedensohler, A., and Herrmann, H.: Particle characterization at the Cape Verde atmospheric observatory during the 2007 RHaMBLe intensive, Atmos. Chem. Phys., 10, 2709–2721, https://doi.org/10.5194/acp-10-2709-2010, 2010.

Norris, S. J., Brooks, I. M., de Leeuw, G., Sirevaag, A., Leck, C., Brooks, B. J., Birch, C. E., and Tjernström, M.: Measurements of bubble size spectra within leads in the Arctic summer pack ice, Ocean Sci., 7, 129–139, https://doi.org/10.5194/os-7-129-2011, 2011.

Notz, D. and Worster, M. G.: Desalination processes of sea ice revisited, J. Geophys. Res.-Oceans, 114, C05006, https://doi.org/10.1029/2008JC004885, 2009.

Obernosterer, I., Catala, P., Lami, R., Caparros, J., Ras, J., Bricaud, A., Dupuy, C., van Wambeke, F., and Lebaron, P.: Biochemical characteristics and bacterial community structure of the sea sur-

face microlayer in the South Pacific Ocean, Biogeosciences, 5, 693–705, https://doi.org/10.5194/bg-5-693-2008, 2008.

O'Dowd, C. D., Facchini, M. C., Cavalli, F., Ceburnis, D., Mircea, M., Decesari, S., Fuzzi, S., Yoon, Y. J., and Putaud, J.-P.: Biogenically driven organic contribution to marine aerosol, Nature, 431, 676–680, https://doi.org/10.1038/nature02959, 2004.

Orellana, M. V., Matrai, P. A., Leck, C., Rauschenberg, C. D., Lee, A. M., and Coz, E.: Marine microgels as a source of cloud condensation nuclei in the high Arctic, P. Natl. Acad. Sci. USA, 108, 13612–13617, https://doi.org/10.1073/pnas.1102457108, 2011.

Panagiotopoulos, C. and Sempéré, R.: Analytical methods for the determination of sugars in marine samples: A historical perspective and future directions, Limnol. Oceanogr.-Meth., 3, 419–454, https://doi.org/10.4319/lom.2005.3.419, 2005.

Papakonstantinou-Presvelou, I., Sourdeval, O., and Quaas, J.: Strong Ocean/Sea-Ice Contrasts Observed in Satellite-Derived Ice Crystal Number Concentrations in Arctic Ice Boundary-Layer Clouds, Geophys. Res. Lett., 49, e2022GL098207, https://doi.org/10.1029/2022GL098207, 2022.

Passow, U.: Transparent exopolymer particles (TEP) in aquatic environments, Prog. Oceanogr., 55, 287–333, https://doi.org/10.1016/S0079-6611(02)00138-6, 2002.

Penner, J. E., Andreae, M. O., Annegarn, H., Barrie, L., Feichter, J., Hegg, D., Jayaraman, A., Leaitch, R., Murphy, D., Nganga, J., and Pitari, G.: Aerosols, their Direct and Indirect Effects, Climate Change 2001: The Scientific Basis. Contribution of Working Group I to the Third Assessment Report of the Intergovernmental Panel on Climate Change, 289–348, https://pure.mpg.de/pubman/faces/ViewItemOverviewPage.jsp?itemId=item_1831230 (last access: 25 May 2023), 2001.

Phongphattarawat, S.: Variability in pigment composition and bio-optical characteristics of phytoplankton populations in the Atlantic basin, University of Oxford, http://purl.org/dc/dcmitype/Text (last access: 25 May 2023), 2016.

Piontek, J., Lunau, M., Händel, N., Borchard, C., Wurst, M., and Engel, A.: Acidification increases microbial polysaccharide degradation in the ocean, Biogeosciences, 7, 1615–1624, https://doi.org/10.5194/bg-7-1615-2010, 2010.

Porter, G. C. E., Adams, M. P., Brooks, I. M., Ickes, L., Karlsson, L., Leck, C., Salter, M. E., Schmale, J., Siegel, K., Sikora, S. N. F., Tarn, M. D., Vüllers, J., Wernli, H., Zieger, P., Zinke, J., and Murray, B. J.: Highly Active Ice-Nucleating Particles at the Summer North Pole, J. Geophys. Res.-Atmos., 127, e2021JD036059, https://doi.org/10.1029/2021JD036059, 2022.

Prather, K. A., Bertram, T. H., Grassian, V. H., Deane, G. B., Stokes, M. D., DeMott, P. J., Aluwihare, L. I., Palenik, B. P., Azam, F., Seinfeld, J. H., Moffet, R. C., Molina, M. J., Cappa, C. D., Geiger, F. M., Roberts, G. C., Russell, L. M., Ault, A. P., Baltrusaitis, J., Collins, D. B., Corrigan, C. E., Cuadra-Rodriguez, L. A., Ebben, C. J., Forestieri, S. D., Guasco, T. L., Hersey, S. P., Kim, M. J., Lambert, W. F., Modini, R. L., Mui, W., Pedler, B. E., Ruppel, M. J., Ryder, O. S., Schoepp, N. G., Sullivan, R. C., and Zhao, D.: Bringing the ocean into the laboratory to probe the chemical complexity of sea spray aerosol, P. Natl. Acad. Sci. USA, 110, 7550–7555, https://doi.org/10.1073/pnas.1300262110, 2013.

Qin, G., Zhu, L., Chen, X., Wang, P. G., and Zhang, Y.: Structural characterization and ecological roles of a novel exopolysaccharide from the deep-sea psychrotolerant bacterium *Pseudoalteromonas* sp. SM9913, Microbiology, 153, 1566–1572, https://doi.org/10.1099/mic.0.2006/003327-0, 2007.

Quinn, P. K., Collins, D. B., Grassian, V. H., Prather, K. A., and Bates, T. S.: Chemistry and Related Properties of Freshly Emitted Sea Spray Aerosol, Chem. Rev., 115, 4383–4399, https://doi.org/10.1021/cr500713g, 2015.

Rastelli, E., Corinaldesi, C., Dell'Anno, A., Lo Martire, M., Greco, S., Cristina Facchini, M., Rinaldi, M., O'Dowd, C., Ceburnis, D., and Danovaro, R.: Transfer of labile organic matter and microbes from the ocean surface to the marine aerosol: an experimental approach, Sci. Rep., 7, 1–10, https://doi.org/10.1038/s41598-017-10563-z, 2017.

Rérolle, V., Ruiz-Pino, D., Rafizadeh, M., Loucaides, S., Papadimitriou, S., Mowlem, M., and Chen, J.: Measuring pH in the Arctic Ocean: Colorimetric method or SeaFET?, Meth. Oceanogr., 17, 32–49, https://doi.org/10.1016/j.mio.2016.05.006, 2016.

Robinson, T.-B., Wurl, O., Bahlmann, E., Jürgens, K., and Stolle, C.: Rising bubbles enhance the gelatinous nature of the air–sea interface, Limnol. Oceanogr., 64, 2358–2372, https://doi.org/10.1002/lno.11188, 2019.

Rolph, R. J., Feltham, D. L., and Schröder, D.: Changes of the Arctic marginal ice zone during the satellite era, The Cryosphere, 14, 1971–1984, https://doi.org/10.5194/tc-14-1971-2020, 2020.

Röttgers, R., McKee, D., and Utschig, C.: Temperature and salinity correction coefficients for light absorption by water in the visible to infrared spectral region, Opt. Express, 22, 25093–25108, https://doi.org/10.1364/OE.22.025093, 2014.

Röttgers, R., Doxaran, D., and Dupouy, C.: Quantitative filter technique measurements of spectral light absorption by aquatic particles using a portable integrating cavity absorption meter (QFT-ICAM), Opt. Express, 24, A1–A20, https://doi.org/10.1364/OE.24.0000A1, 2016.

Russell, L. M., Hawkins, L. N., Frossard, A. A., Quinn, P. K., and Bates, T. S.: Carbohydrate-like composition of submicron atmospheric particles and their production from ocean bubble bursting, P. Natl. Acad. Sci. USA, 107, 6652–6657, https://doi.org/10.1073/pnas.0908905107, 2010.

Šantl-Temkiv, T., Gosewinkel, U., Starnawski, P., Lever, M., and Finster, K.: Aeolian dispersal of bacteria in southwest Greenland: their sources, abundance, diversity and physiological states, FEMS Microbiol. Ecol., 94, fiy031, https://doi.org/10.1093/femsec/fiy031, 2018.

Šantl-Temkiv, T., Sikoparija, B., Maki, T., Carotenuto, F., Amato, P., Yao, M., Morris, C. E., Schnell, R., Jaenicke, R., Pöhlker, C., DeMott, P. J., Hill, T. C. J., and Huffman, J. A.: Bioaerosol field measurements: Challenges and perspectives in outdoor studies, Aerosol Sci. Tech., 54, 520–546, https://doi.org/10.1080/02786826.2019.1676395, 2020.

Schiffer, J. M., Mael, L. E., Prather, K. A., Amaro, R. E., and Grassian, V. H.: Sea Spray Aerosol: Where Marine Biology Meets Atmospheric Chemistry, ACS Cent. Sci., 4, 1617–1623, https://doi.org/10.1021/acscentsci.8b00674, 2018.

Schill, S. R., Burrows, S. M., Hasenecz, E. S., Stone, E. A., and Bertram, T. H.: The Impact of Divalent Cations on the Enrichment of Soluble Saccharides in Primary Sea Spray Aerosol, Atmosphere, 9, 476, https://doi.org/10.3390/atmos9120476, 2018.

Schmale, J., Zieger, P., and Ekman, A. M. L.: Aerosols in current and future Arctic climate, Nat. Clim. Change, 11, 95–105, https://doi.org/10.1038/s41558-020-00969-5, 2021.

Schmithüsen, H.: Continuous meteorological surface measurement during POLARSTERN cruise PS106/1 (ARK-XXXI/1.1), PANGAEA [data set], https://doi.org/10.1594/PANGAEA.886302, 2018.

Schmithüsen, H.: Continuous meteorological surface measurement during POLARSTERN cruise PS106/2 (ARK-XXXI/1.2), PANGAEA [data set], https://doi.org/10.1594/PANGAEA.901179, 2019.

Schmitt-Kopplin, P., Liger-Belair, G., Koch, B. P., Flerus, R., Kattner, G., Harir, M., Kanawati, B., Lucio, M., Tziotis, D., Hertkorn, N., and Gebefügi, I.: Dissolved organic matter in sea spray: a transfer study from marine surface water to aerosols, Biogeosciences, 9, 1571–1582, https://doi.org/10.5194/bg-9-1571-2012, 2012.

Sellegri, K., O'Dowd, C. D., Yoon, Y. J., Jennings, S. G., and Leeuw, G. de: Surfactants and submicron sea spray generation, J. Geophys. Res.-Atmos., 111, D22215, https://doi.org/10.1029/2005JD006658, 2006.

Spencer, R. G. M., Aiken, G. R., Butler, K. D., Dornblaser, M. M., Striegl, R. G., and Hernes, P. J.: Utilizing chromophoric dissolved organic matter measurements to derive export and reactivity of dissolved organic carbon exported to the Arctic Ocean: A case study of the Yukon River, Alaska, Geophys. Res. Lett., 36, L06401, https://doi.org/10.1029/2008GL036831, 2009.

Stedmon, C. A., Amon, R. M. W., Rinehart, A. J., and Walker, S. A.: The supply and characteristics of colored dissolved organic matter (CDOM) in the Arctic Ocean: Pan Arctic trends and differences, Mar. Chem., 124, 108–118, https://doi.org/10.1016/j.marchem.2010.12.007, 2011.

Stein, A. F., Draxler, R. R., Rolph, G. D., Stunder, B. J. B., Cohen, M. D., and Ngan, F.: NOAA's HYSPLIT Atmospheric Transport and Dispersion Modeling System, B. Am. Meteorol. Soc., 96, 2059–2077, https://doi.org/10.1175/BAMS-D-14-00110.1, 2015.

Stolle, C., Nagel, K., Labrenz, M., and Jürgens, K.: Succession of the sea-surface microlayer in the coastal Baltic Sea under natural and experimentally induced low-wind conditions, Biogeosciences, 7, 2975–2988, https://doi.org/10.5194/bg-7-2975-2010, 2010.

Strong, C. and Rigor, I. G.: Arctic marginal ice zone trending wider in summer and narrower in winter, Geophys. Res. Lett., 40, 4864–4868, https://doi.org/10.1002/grl.50928, 2013.

Sud, I. J. and Tyler, M. E.: Cell-Wall Composition and Osmotic Fragility of Selected Marine Bacteria, J. Bacteriol., 87, 696–700, 1964.

Suzuki, E. and Suzuki, R.: Variation of Storage Polysaccharides in Phototrophic Microorganisms, Journal of Applied Glycoscience, 60, 21–27, https://doi.org/10.5458/jag.jag.JAG-2012_016, 2013.

Taylor, B. B., Torrecilla, E., Bernhardt, A., Taylor, M. H., Peeken, I., Röttgers, R., Piera, J., and Bracher, A.: Bio-optical provinces in the eastern Atlantic Ocean and their biogeographical relevance, Biogeosciences, 8, 3609–3629, https://doi.org/10.5194/bg-8-3609-2011, 2011.

Thomson, J.: Wave propagation in the marginal ice zone: connections and feedback mechanisms within the air–ice–ocean system, Philos. T. R. Soc. A, 380, 20210251, https://doi.org/10.1098/rsta.2021.0251, 2022.

Triesch, N., van Pinxteren, M., Engel, A., and Herrmann, H.: Concerted measurements of free amino acids at the Cabo Verde islands: high enrichments in submicron sea spray aerosol particles and cloud droplets, Atmos. Chem. Phys., 21, 163–181, https://doi.org/10.5194/acp-21-163-2021, 2021a.

Triesch, N., van Pinxteren, M., Frka, S., Stolle, C., Spranger, T., Hoffmann, E. H., Gong, X., Wex, H., Schulz-Bull, D., Gašparović, B., and Herrmann, H.: Concerted measurements of lipids in seawater and on submicrometer aerosol particles at the Cabo Verde islands: biogenic sources, selective transfer and high enrichments, Atmos. Chem. Phys., 21, 4267–4283, https://doi.org/10.5194/acp-21-4267-2021, 2021b.

Triesch, N., van Pinxteren, M., Salter, M., Stolle, C., Pereira, R., Zieger, P., and Herrmann, H.: Sea Spray Aerosol Chamber Study on Selective Transfer and Enrichment of Free and Combined Amino Acids, ACS Earth Space Chem., 5, 1564–1574, https://doi.org/10.1021/acsearthspacechem.1c00080, 2021c.

Trueblood, J. V., Wang, X., Or, V. W., Alves, M. R., Santander, M. V., Prather, K. A., and Grassian, V. H.: The Old and the New: Aging of Sea Spray Aerosol and Formation of Secondary Marine Aerosol through OH Oxidation Reactions, ACS Earth Space Chem., 3, 2307–2314, https://doi.org/10.1021/acsearthspacechem.9b00087, 2019.

Tynan, E., Clarke, J. S., Humphreys, M. P., Ribas-Ribas, M., Esposito, M., Rérolle, V. M. C., Schlosser, C., Thorpe, S. E., Tyrrell, T., and Achterberg, E. P.: Physical and biogeochemical controls on the variability in surface pH and calcium carbonate saturation states in the Atlantic sectors of the Arctic and Southern Oceans, Deep-Sea Res. Pt. II, 127, 7–27, https://doi.org/10.1016/j.dsr2.2016.01.001, 2016.

Uetake, J., Hill, T. C. J., Moore, K. A., DeMott, P. J., Protat, A., and Kreidenweis, S. M.: Airborne bacteria confirm the pristine nature of the Southern Ocean boundary layer, P. Natl. Acad. Sci, USA, 117, 13275–13282, https://doi.org/10.1073/pnas.2000134117, 2020.

van Pinxteren, M., Müller, C., Iinuma, Y., Stolle, C., and Herrmann, H.: Chemical Characterization of Dissolved Organic Compounds from Coastal Sea Surface Microlayers (Baltic Sea, Germany), Environ. Sci. Technol., 46, 10455–10462, https://doi.org/10.1021/es204492b, 2012.

van Pinxteren, M., Barthel, S., Fomba, K. W., Müller, K., Von Tümpling, W., and Herrmann, H.: The influence of environmental drivers on the enrichment of organic carbon in the sea surface microlayer and in submicron aerosol particles – measurements from the Atlantic Ocean, Elem. Sci. Anth., 5, 35, https://doi.org/10.1525/elementa.225, 2017.

van Pinxteren, M., Robinson, T.-B., Zeppenfeld, S., Gong, X., Bahlmann, E., Fomba, K. W., Triesch, N., Stratmann, F., Wurl, O., Engel, A., Wex, H., and Herrmann, H.: High number concentrations of transparent exopolymer particles in ambient aerosol particles and cloud water – a case study at the tropical Atlantic Ocean, Atmos. Chem. Phys., 22, 5725–5742, https://doi.org/10.5194/acp-22-5725-2022, 2022.

van Pinxteren, M., Zeppenfeld, S., Fomba, K. W., Triesch, N., Frka, S., and Herrmann, H.: Amino acids, carbohydrates, and lipids in the tropical oligotrophic Atlantic Ocean: sea-to-air transfer and

atmospheric in situ formation, Atmos. Chem. Phys., 23, 6571–6590, https://doi.org/10.5194/acp-23-6571-2023, 2023.

Vaqué, D., Boras, J. A., Arrieta, J. M., Agustí, S., Duarte, C. M., and Sala, M. M.: Enhanced Viral Activity in the Surface Microlayer of the Arctic and Antarctic Oceans, Microorganisms, 9, 317, https://doi.org/10.3390/microorganisms9020317, 2021.

Veron, F.: Ocean Spray, Annu. Rev. Fluid Mech., 47, 507–538, https://doi.org/10.1146/annurev-fluid-010814-014651, 2015.

Walker, S. A., Amon, R. M. W., and Stedmon, C. A.: Variations in high-latitude riverine fluorescent dissolved organic matter: A comparison of large Arctic rivers, J. Geophys. Res.-Biogeo., 118, 1689–1702, https://doi.org/10.1002/2013JG002320, 2013.

Wang, X., Deane, G. B., Moore, K. A., Ryder, O. S., Stokes, M. D., Beall, C. M., Collins, D. B., Santander, M. V., Burrows, S. M., Sultana, C. M., and Prather, K. A.: The role of jet and film drops in controlling the mixing state of submicron sea spray aerosol particles, P. Natl. Acad. Sci. USA, 114, 6978–6983, https://doi.org/10.1073/pnas.1702420114, 2017.

Wendisch, M., Macke, A., Ehrlich, A., Lüpkes, C., Mech, M., Chechin, D., Dethloff, K., Barientos, C., Bozem, H., Brückner, M., Clemen, H.-C., Crewell, S., Donth, T., Dupuy, R., Ebell, K., Egerer, U., Engelmann, R., Engler, C., Eppers, O., Gehrmann, M., Gong, X., Gottschalk, M., Gourbeyre, C., Griesche, H., Hartmann, J., Hartmann, M., Heinold, B., Herber, A., Herrmann, H., Heygster, G., Hoor, P., Jafariserajehlou, S., Jäkel, E., Järvinen, E., Jourdan, O., Kästner, U., Kecorius, S., Knudsen, E. M., Köllner, F., Kretzschmar, J., Lelli, L., Leroy, D., Maturilli, M., Mei, L., Mertes, S., Mioche, G., Neuber, R., Nicolaus, M., Nomokonova, T., Notholt, J., Palm, M., van Pinxteren, M., Quaas, J., Richter, P., Ruiz-Donoso, E., Schäfer, M., Schmieder, K., Schnaiter, M., Schneider, J., Schwarzenböck, A., Seifert, P., Shupe, M. D., Siebert, H., Spreen, G., Stapf, J., Stratmann, F., Vogl, T., Welti, A., Wex, H., Wiedensohler, A., Zanatta, M., and Zeppenfeld, S.: The Arctic Cloud Puzzle: Using ACLOUD/PASCAL Multi-Platform Observations to Unravel the Role of Clouds and Aerosol Particles in Arctic Amplification, B. Am. Meteorol. Soc., 100, 841–871, https://doi.org/10.1175/BAMS-D-18-0072.1, 2018.

Wendisch, M., Brückner, M., Crewell, S., Ehrlich, A., Notholt, J., Lüpkes, C., Macke, A., Burrows, J. P., Rinke, A., Quaas, J., Maturilli, M., Schemann, V., Shupe, M. D., Akansu, E. F., Barrientos-Velasco, C., Bärfuss, K., Blechschmidt, A.-M., Block, K., Bougoudis, I., Bozem, H., Böckmann, C., Bracher, A., Bresson, H., Bretschneider, L., Buschmann, M., Chechin, D. G., Chylik, J., Dahlke, S., Deneke, H., Dethloff, K., Donth, T., Dorn, W., Dupuy, R., Ebell, K., Egerer, U., Engelmann, R., Eppers, O., Gerdes, R., Gierens, R., Gorodetskaya, I. V., Gottschalk, M., Griesche, H., Gryanik, V. M., Handorf, D., Harm-Altstädter, B., Hartmann, J., Hartmann, M., Heinold, B., Herber, A., Herrmann, H., Heygster, G., Höschel, I., Hofmann, Z., Hölemann, J., Hünerbein, A., Jafariserajehlou, S., Jäkel, E., Jacobi, C., Janout, M., Jansen, F., Jourdan, O., Jurányi, Z., Kalesse-Los, H., Kanzow, T., Käthner, R., Kliesch, L. L., Klingebiel, M., Knudsen, E. M., Kovács, T., Körtke, W., Krampe, D., Kretzschmar, J., Kreyling, D., Kulla, B., Kunkel, D., Lampert, A., Lauer, M., Lelli, L., Lerber, A. von, Linke, O., Löhnert, U., Lonardi, M., Losa, S. N., Losch, M., Maahn, M., Mech, M., Mei, L., Mertes, S., Metzner, E., Mewes, D., Michaelis, J., Mioche, G., Moser, M., Nakoudi, K., Neggers, R., Neuber, R., Nomokonova, T., Oelker, J., Papakonstantinou-Presvelou, I., et al.: Atmospheric and Surface Processes, and Feedback Mechanisms Determining Arctic Amplification: A Review of First Results and Prospects of the (AC)3 Project, B. Am. Meteorol. Soc., 104, E208–E242, https://doi.org/10.1175/BAMS-D-21-0218.1, 2023.

Wietz, M., Wemheuer, B., Simon, H., Giebel, H.-A., Seibt, M. A., Daniel, R., Brinkhoff, T., and Simon, M.: Bacterial community dynamics during polysaccharide degradation at contrasting sites in the Southern and Atlantic Oceans, Environ. Microbiol., 17, 3822–3831, https://doi.org/10.1111/1462-2920.12842, 2015.

Wilbourn, E. K., Thornton, D. C. O., Ott, C., Graff, J., Quinn, P. K., Bates, T. S., Betha, R., Russell, L. M., Behrenfeld, M. J., and Brooks, S. D.: Ice Nucleation by Marine Aerosols Over the North Atlantic Ocean in Late Spring, J. Geophys. Res.-Atmos., 125, e2019JD030913, https://doi.org/10.1029/2019JD030913, 2020.

Williams, P. M., Carlucci, A. F., Henrichs, S. M., Van Vleet, E. S., Horrigan, S. G., Reid, F. M. H., and Robertson, K. J.: Chemical and microbiological studies of sea-surface films in the Southern Gulf of California and off the West Coast of Baja California, Mar. Chem., 19, 17–98, https://doi.org/10.1016/0304-4203(86)90033-2, 1986.

Wurl, O., Miller, L., Röttgers, R., and Vagle, S.: The distribution and fate of surface-active substances in the sea-surface microlayer and water column, Mar. Chem., 115, 1–9, https://doi.org/10.1016/j.marchem.2009.04.007, 2009.

Wurl, O., Miller, L., and Vagle, S.: Production and fate of transparent exopolymer particles in the ocean, J. Geophys. Res.-Oceans, 116, C00H13, https://doi.org/10.1029/2011JC007342, 2011.

Xu, M., Tsona Tchinda, N., Li, J., and Du, L.: Insoluble lipid film mediates transfer of soluble saccharides from the sea to the atmosphere: the role of hydrogen bonding, Atmos. Chem. Phys., 23, 2235–2249, https://doi.org/10.5194/acp-23-2235-2023, 2023.

Xu, W., Ovadnevaite, J., Fossum, K. N., Lin, C., Huang, R.-J., Ceburnis, D., and O'Dowd, C.: Sea spray as an obscured source for marine cloud nuclei, Nat. Geosci., 15, 282–286, https://doi.org/10.1038/s41561-022-00917-2, 2022.

Yang, X., Pyle, J. A., and Cox, R. A.: Sea salt aerosol production and bromine release: Role of snow on sea ice, Geophys. Res. Lett., 35, L16815, https://doi.org/10.1029/2008GL034536, 2008.

Zábori, J., Matisāns, M., Krejci, R., Nilsson, E. D., and Ström, J.: Artificial primary marine aerosol production: a laboratory study with varying water temperature, salinity, and succinic acid concentration, Atmos. Chem. Phys., 12, 10709–10724, https://doi.org/10.5194/acp-12-10709-2012, 2012.

Zäncker, B., Bracher, A., Röttgers, R., and Engel, A.: Variations of the Organic Matter Composition in the Sea Surface Microlayer: A Comparison between Open Ocean, Coastal, and Upwelling Sites Off the Peruvian Coast, Front. Microbiol., 8, 2369, https://doi.org/10.3389/fmicb.2017.02369, 2017.

Zäncker, B., Cunliffe, M., and Engel, A.: Eukaryotic community composition in the sea surface microlayer across an east–west transect in the Mediterranean Sea, Biogeosciences, 18, 2107–2118, https://doi.org/10.5194/bg-18-2107-2021, 2021.

Zeppenfeld, S.: Daily sea ice maps for PS106 showing sea ice concentrations (SIC) and 120 h back trajectories on an hourly basis at three arrival heights (red: 50 m, purple: 250 m and pink: 1000 m), TIB AV-Portal [video], https://doi.org/10.5446/62589, 2023.

Zeppenfeld, S., van Pinxteren, M., Hartmann, M., Bracher, A., Stratmann, F., and Herrmann, H.: Glucose as a Potential Chem-

ical Marker for Ice Nucleating Activity in Arctic Seawater and Melt Pond Samples, Environ. Sci. Technol., 53, 8747–8756, https://doi.org/10.1021/acs.est.9b01469, 2019a.

Zeppenfeld, S., van Pinxteren, M., Hartmann, M., Bracher, A., Wiegmann, S., Stratmann, F., and Herrmann, H.: Glucose, T50 and salinity in the surface microlayer and bulk water samples from the Arctic during POLARSTERN cruise PS106 (2017), PANGAEA [data set], https://doi.org/10.1594/PANGAEA.899258, 2019b.

Zeppenfeld, S., van Pinxteren, M., Engel, A., and Herrmann, H.: A protocol for quantifying mono- and polysaccharides in seawater and related saline matrices by electro-dialysis (ED) – combined with HPAEC-PAD, Ocean Sci., 16, 817–830, https://doi.org/10.5194/os-16-817-2020, 2020.

Zeppenfeld, S., van Pinxteren, M., van Pinxteren, D., Wex, H., Berdalet, E., Vaqué, D., Dall'Osto, M., and Herrmann, H.: Aerosol Marine Primary Carbohydrates and Atmospheric Transformation in the Western Antarctic Peninsula, ACS Earth Space Chem., 5, 1032–1047, https://doi.org/10.1021/acsearthspacechem.0c00351, 2021a.

Zeppenfeld, S., Fuchs, S., Rödger, S., Dietze, A., van Pinxteren, M., and Herrmann, H.: Marine carbohydrates and inorganic ions in size-resolved atmospheric particles collected over the Southern Ocean, PANGAEA [data set], https://doi.org/10.1594/PANGAEA.927565, 2021b.

Zeppenfeld, S., van Pinxteren, M., Fuchs, S., Hartmann, M., Gong, X., and Herrmann, H.: Inorganic ions in fog water sampled from the Arctic in 2017, PANGAEA [data set], https://doi.org/10.1594/PANGAEA.932573, 2021c.

Zeppenfeld, S., van Pinxteren, M., Fuchs, S., Hartmann, M., Gong, X., and Herrmann, H.: Inorganic ions in size-resolved aerosol particles sampled from the Arctic in 2017, PANGAEA [data set], https://doi.org/10.1594/PANGAEA.932569, 2021d.

Zeppenfeld, S., van Pinxteren, M., Fuchs, S., Hartmann, M., and Herrmann, H.: Combined carbohydrates, dissolved free carbohydrates and pH in Arctic fog water sampled during PS106, PANGAEA [data set], https://doi.org/10.1594/PANGAEA.962208, 2023a.

Zeppenfeld, S., van Pinxteren, M., Fuchs, S., Hartmann, M., and Herrmann, H.: Combined carbohydrates, organic carbon and total aerosol mass concentrations in size-resolved aerosol particles sampled from the Arctic in 2017, PANGAEA [data set], https://doi.org/10.1594/PANGAEA.962210, 2023b.

Zeppenfeld, S., Bracher, A., Wiegmann, S., Zeising, M., Fuchs, S., van Pinxteren, M., and Herrmann, H.: Dissolved and particulate combined carbohydrates, pH, inorganic ions, CDOM and particulate absorption of SML and bulk water in Arctic surface seawater and melt ponds, PANGAEA [data set], https://doi.org/10.1594/PANGAEA.961004, 2023c.

Zinke, J., Salter, M. E., Leck, C., Lawler, M. J., Porter, G. C. E., Adams, M. P., Brooks, I. M., Murray, B. J., and Zieger, P.: The development of a miniaturised balloon-borne cloud water sampler and its first deployment in the high Arctic, Tellus B, 73, 1–12, https://doi.org/10.1080/16000889.2021.1915614, 2021.